

# A first taste of nonlinear beam dynamics

Hannes Bartosik<sup>†</sup>, Yannis Papaphilippou<sup>†</sup>, Andrzej Wolski<sup>‡</sup>

<sup>†</sup>CERN, Geneva, Switzerland,

<sup>‡</sup>University of Liverpool, and the Cockcroft Institute, UK

## Abstract

Nonlinear dynamics can impact the performance of a particle accelerator in a number of different ways, depending on the type of the accelerator and the parameter regime in which it operates. Effects can range from minor changes in beam properties or behaviour, to serious limitations on beam stability and machine performance. In these notes, we provide a brief introduction to nonlinear dynamics in accelerators. After a review of some relevant results from linear dynamics, we outline some of the main ideas of nonlinear dynamics, framing the discussion in the context of two examples of different types of accelerator: a single-pass system (a bunch compressor) and a periodic system (a storage ring). We show how an understanding of the origins and nature of the nonlinear behaviour, together with the use of appropriate analysis tools, can prove useful in predicting the effects of nonlinear dynamics in different systems, and allow the design of appropriate corrections or mitigations.

## 1 Introduction

In these notes on nonlinear dynamics in particle accelerators, we shall discuss a number of topics:

- effects of nonlinear perturbations in single-pass and periodic systems, including phase space distortions, resonances, tune shifts and dynamic aperture limitations;
- mathematical tools for modelling nonlinear dynamics, including power series maps and symplectic maps;
- analysis methods such as normal form analysis and frequency map analysis.

Our goal is not to provide a rigorous or comprehensive review of nonlinear dynamics in accelerators (which is a very large subject), but to provide a short introduction to some of the key concepts and phenomena. The topics that we discuss are covered in many publications: some suggestions for further reading, where specific topics that may be of interest are covered in greater depth, are given in section 7. We shall frame our discussion in the context of two types of accelerator system: first, a bunch compressor (a single-pass system), and later, a storage ring (a multi-turn system). To begin with, however, we briefly review some of the principles of linear dynamics in particle accelerators, that form an important foundation for the development of ideas in nonlinear dynamics.

## 2 Foundations from linear dynamics

Particle motion through simple components such as drifts, dipoles and quadrupoles can be represented by *linear transfer maps*<sup>1</sup>. For example, in a drift space, the horizontal co-ordinate  $x$  and momentum  $p_x$  change from initial values  $x_0$  and  $p_{x0}$  at the entrance to the drift space, to final values  $x_1$  and  $p_{x1}$  at the exit, given by:

$$x_1 = x_0 + Lp_{x0}, \tag{1}$$

$$p_{x1} = p_{x0}, \tag{2}$$

<sup>1</sup>Linear dynamics is covered in many standard texts in accelerator physics, for example [1–3].

where  $L$  is the length of the drift space. Note that the horizontal (canonical) momentum is given by:

$$p_x = \frac{\gamma m v_x}{P_0}, \quad (3)$$

where  $\gamma$  is the relativistic factor,  $m$  is the rest mass of the particle,  $v_x$  is the horizontal velocity, and  $P_0$  is the reference momentum. The reference momentum is a fixed value (in the absence of acceleration) that is used mainly for convenience, for scaling quantities such as the particle momentum. In principle, the reference momentum can be chosen arbitrarily, though it is usually best to choose a value equal to the “design” momentum of the beam. For small values of  $p_x$  (i.e. for  $|p_x| \ll 1$ ), the horizontal momentum is approximately equal to the angle of the trajectory with respect to the design trajectory:

$$p_x \approx \frac{dx}{ds}. \quad (4)$$

The reference trajectory is simply a line through space that acts as the origin of the local cartesian coordinate system, with (transverse) axes  $x$  horizontally and  $y$  vertically. The variable  $s$  is the distance along the reference trajectory from a fixed starting point.

Linear transfer maps can be written in terms of matrices. For example, for a drift space of length  $L$ , the map given by equations (1) and (2) can be written:

$$\begin{pmatrix} x_1 \\ p_{x1} \end{pmatrix} = \begin{pmatrix} 1 & L \\ 0 & 1 \end{pmatrix} \begin{pmatrix} x_0 \\ p_{x0} \end{pmatrix}. \quad (5)$$

In general, a linear transformation can be written:

$$\vec{x}_1 = R \vec{x}_0 + \vec{A}, \quad (6)$$

where  $\vec{x}_0$  and  $\vec{x}_1$  are the initial and final phase space vectors, with components  $(x_0, p_{x0})$  and  $(x_1, p_{x1})$ , respectively,  $R$  is a matrix (the *transfer matrix*) and  $\vec{A}$  is a vector. The components of  $R$  and  $\vec{A}$  are constant, i.e. they do not depend on  $\vec{x}_0$ : it is this feature that makes the map (6) a *linear* map.

In the case that  $\vec{A} = 0$  for all elements in a beamline, the transfer matrix for that beamline can be found simply by multiplying the transfer matrices for the accelerator components within that beamline. For example, if a beamline consists of a sequence of elements with transfer matrices  $R_1, R_2, R_3 \dots R_n$ , with the beam passing through the elements in that order, then after the first element, the phase space vector becomes:

$$\vec{x}_1 = R_1 \vec{x}_0. \quad (7)$$

After the second element, it becomes:

$$\vec{x}_2 = R_2 \vec{x}_1 = R_2 R_1 \vec{x}_0. \quad (8)$$

Eventually, after  $n$  elements, the phase space vector is:

$$\vec{x}_n = R_{\text{total}} \vec{x}_0 = R_n R_{n-1} \dots R_2 R_1 \vec{x}_0. \quad (9)$$

The transfer matrix  $R_{\text{total}}$  is constructed by multiplying the transfer matrices for the individual elements, writing them in the multiplication in the reverse order that they appear in the beamline.

For a periodic beamline (i.e. a beamline constructed from a repeated unit) the transfer matrix for a single period can be parameterised in terms of the Courant–Snyder parameters  $(\alpha_x, \beta_x, \gamma_x)$  and the phase advance,  $\mu_x$ :

$$R = \begin{pmatrix} \cos(\mu_x) + \alpha_x \sin(\mu_x) & \beta_x \sin(\mu_x) \\ -\gamma_x \sin(\mu_x) & \cos(\mu_x) - \alpha_x \sin(\mu_x) \end{pmatrix}. \quad (10)$$

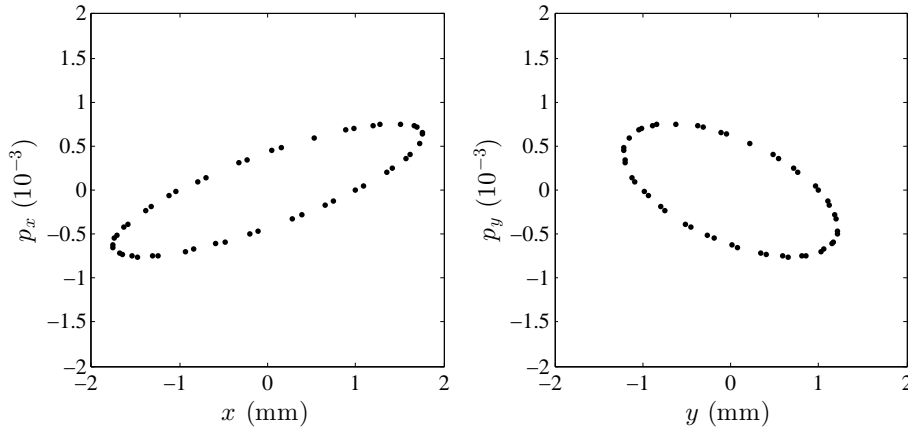


**Fig. 1:** Horizontal and vertical phase space portraits for a particle moving along a periodic beamline. Each point indicates the co-ordinate and corresponding component of the momentum of the particle after each full pass through a periodic section of the beamline. Since the beamline is linear and stable, the points lie on ellipses with shapes determined by the Courant–Snyder parameters for the beamline. The area of the ellipse is determined by the betatron amplitude of the particle in each plane. The angle around the ellipse that the particle moves in each period corresponds to the phase advance.

If the transfer matrix is found by multiplying together the transfer matrices for the elements in a unit cell (in the appropriate order), then the values of the Courant–Snyder parameters and the phase advance  $\mu_x$  can be found by equating the components of the matrix in terms of the beamline elements with the components of the matrix given in the form (10).

Neglecting synchrotron radiation and various collective effects, the transfer matrices will be *symplectic*. For a  $2 \times 2$  matrix, this means that the matrix will have unit determinant, which leads to the condition:

$$\beta_x \gamma_x - \alpha_x^2 = 1. \quad (11)$$

If the beamline is stable, then the characteristics of the particle motion can be represented by a *phase space portrait* showing the co-ordinates and momenta of a particle after an increasing number of passes through successive periods of the beamline. If the transfer map for each period is linear, then the phase space portrait is an ellipse with area  $\pi J_x$ : examples (for horizontal and vertical motion) are shown in Fig. 1. The quantity  $J_x$  is called the *betatron action*, and characterises the amplitude of the betatron oscillations. The shape of the ellipse is described by the Courant–Snyder parameters, as shown in Fig. 2. The rate at which particles move around the ellipse corresponds to the phase advance in each periodic section of the beamline, and (for linear motion) is independent of the betatron action.

The betatron action  $J_x$  and the phase (or angle)  $\phi_x$  provide an alternative to the regular cartesian variables  $x, p_x$  for describing the motion of particles in an accelerator beamline. The cartesian variables can be expressed in terms of the action–angle variables:

$$x = \sqrt{2\beta_x J_x} \cos(\phi_x), \quad (12)$$

$$p_x = -\sqrt{\frac{2J_x}{\beta_x}} (\sin(\phi_x) + \alpha_x \cos(\phi_x)). \quad (13)$$

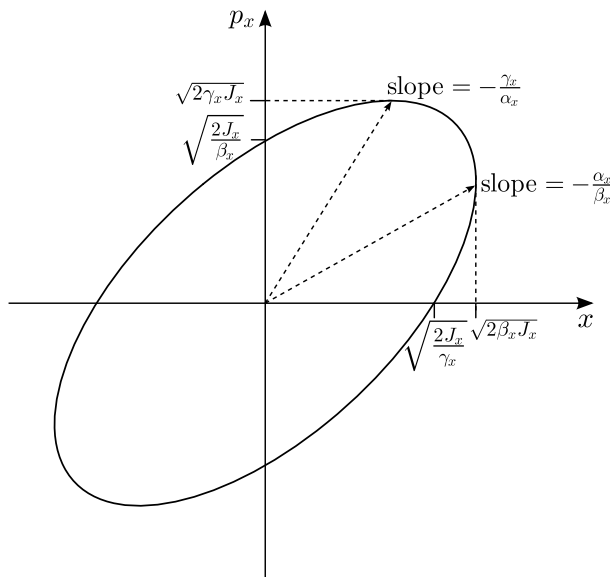


**Fig. 2:** The Courant–Snyder parameters describe the shape of the ellipse mapped out in phase space as a particle moves through successive periods in a periodic beamline. The area of the ellipse, corresponding to the betatron amplitude, is  $\pi J_x$ , where  $J_x$  is the betatron action.

### 3 From linear to nonlinear maps

Nonlinearities in the particle dynamics can come from a number of different sources, including: stray fields in drift spaces; higher-order multipole components in dipoles and quadrupoles; higher-order multipole magnets (sextupoles, octupoles etc.) used to control various properties of the beam; effects of fields generated by a bunch of particles on individual particles within the bunch (space-charge forces, beam-beam effects, and many others). The extent to which each of these (or other) sources contributes to nonlinear effects in an accelerator depends very much on the specific case.

The effects of nonlinearities can be varied and quite dramatic, and can impact the operation and overall performance of an accelerator in many different ways. It is important to have some understanding of nonlinear dynamics for optimising the design and operation of many accelerator systems. It is also important to have the appropriate mathematical tools and techniques for the analysis of nonlinear dynamics, and a range of powerful methods have been developed over the years. We shall mention a few of these methods in a later section, but one of the simplest approaches is to write the transfer map as a power series in the dynamical variables: this is a natural extension of linear transfer maps, given (for example) in a drift space in Eqs. (1) and (2). As an example of this approach, consider a particle moving through a sextupole magnet. The vertical component of the field in a sextupole is given by:

$$\frac{B_y}{B\rho} = \frac{1}{2}k_2x^2, \quad (14)$$

where  $B\rho = P_0/q$  is the beam rigidity, and  $k_2$  is the normalised sextupole gradient. In the “thin lens” approximation, the horizontal deflection of a particle on passing through the sextupole is:

$$\Delta p_x = -\frac{1}{B\rho} \int B_y ds \approx -\frac{1}{2}k_2Lx^2, \quad (15)$$

where  $L$  is the length of the sextupole. Hence, the transfer map for a sextupole in the thin lens approximation is:

$$x_1 = x_0, \quad (16)$$

$$p_{x1} = p_{x0} - \frac{1}{2}k_2 L x_0^2. \quad (17)$$

Although we can write the effect of the sextupole as a transfer map in the same way that we did for a drift space in Eqs. (1) and (2), in the case of the sextupole, the map is *nonlinear*: it depends on higher-order terms in the original values of the phase space variables. This means that the transfer map cannot be written simply as a matrix. However, we can generalise the matrix equation (6), to express a nonlinear transfer map as a power series:

$$x_1 = A_1 + R_{11}x_0 + R_{12}p_{x0} + T_{111}x_0^2 + T_{112}x_0p_{x0} + T_{122}p_{x0}^2 + \dots \quad (18)$$

$$p_{x1} = A_2 + R_{21}x_0 + R_{22}p_{x0} + T_{211}x_0^2 + T_{212}x_0p_{x0} + T_{222}p_{x0}^2 + \dots \quad (19)$$

The coefficients  $R_{ij}$  correspond to components of the transfer matrix  $R$ . The coefficients of higher-order (nonlinear) terms are conventionally represented by  $T_{ijk}$  (second order),  $U_{ijkl}$  (third order) and so on. The values of the indices correspond to the components of the phase space vector, thus:

|             |     |       |     |       |     |          |
|-------------|-----|-------|-----|-------|-----|----------|
| index value | 1   | 2     | 3   | 4     | 5   | 6        |
| component   | $x$ | $p_x$ | $y$ | $p_y$ | $z$ | $\delta$ |

Hence,  $T_{212}$  is the coefficient for a second-order term (three indices), referring specifically to the part of the map for  $p_x$  (first index,  $i = 2$ ), depending on the product of  $x$  (second index,  $j = 1$ ) and  $p_x$  (third index,  $k = 2$ ). Because multiplication is commutative, there is no distinction between (for example)  $T_{212}$  and  $T_{221}$ .

The effects of nonlinearities depend very much on the type of accelerator system being considered. It is often useful, in this context, to make a distinction between periodic beamlines (e.g. in a storage ring) and non-periodic, or single-pass systems. In a periodic beamline, the effects of nonlinearities can include:

- distortion of the shape of the phase space ellipse;
- dependence of the phase advance per period on the betatron amplitude;
- instability of motion at large amplitudes;
- the appearance of features such as “phase space islands” (closed loops around points away from the origin) in the phase space portrait.

Before considering periodic beamlines, however, we shall consider in more detail the effects of nonlinearities in a single-pass beamline. The discussion (in the following section) will be based on the example of a bunch compressor.

#### 4 Nonlinear dynamics in a single-pass beamline: a bunch compressor

As an example of how nonlinear effects can impact the performance of an accelerator, we shall consider a bunch compressor. Bunch compressors reduce the length of a bunch by performing a rotation in longitudinal phase space, and are used, for example, in free electron lasers to increase the peak current.

We first outline the structure of the bunch compressor, and construct the complete transfer map by combining the transfer maps for the different sections. We then specify the parameters of the principal components based on consideration of the linear dynamics and the compression ratio that the bunch compressor should achieve. This provides the basis for an analysis of both linear and nonlinear effects: based on the results of this analysis, the final step is to adjust the parameters, to compensate (as far as possible) the nonlinear effects that may adversely affect the performance of the system.

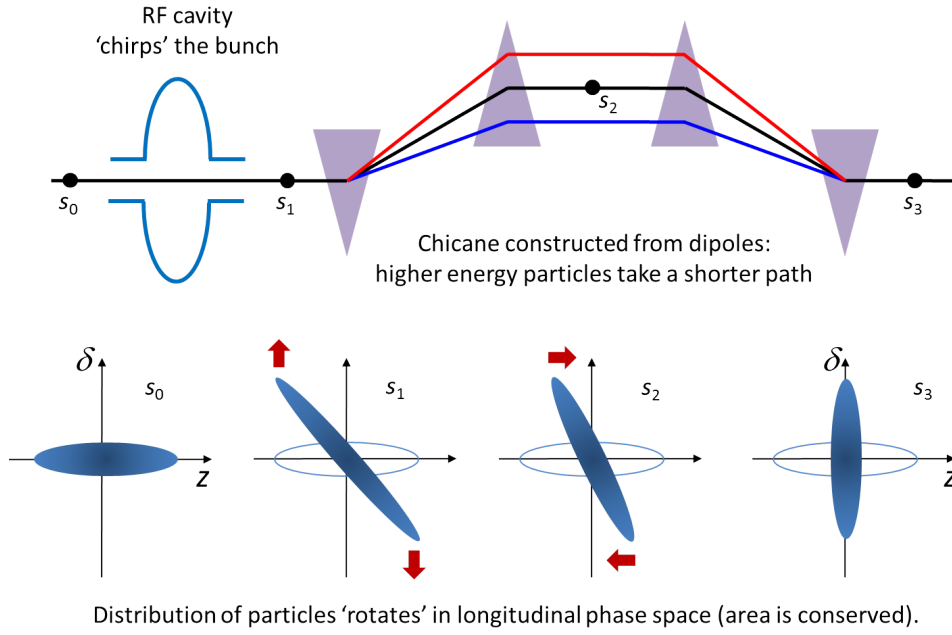


**Fig. 3:** Top: schematic of a bunch compressor. A bunch of particles (moving from left to right along the beamline) first passes through an RF cavity, and then through a sequence of dipoles. Bottom: changes in the distribution of particles in the bunch in longitudinal phase space, indicating the transformations that take place as the bunch moves through the bunch compressor.

#### 4.1 Construction of the transfer map

A schematic of the bunch compressor that we shall use in this example is shown in Fig. 3 (top), and consists of an RF cavity followed by a chicane constructed from four dipoles. The RF cavity is designed to “chirp” the bunch, i.e. to provide a change in energy deviation as a function of longitudinal position  $z$  within the bunch ( $z > 0$  at the head of the bunch). The accelerating field in the cavity varies with time. Suppose that a particle in the centre of the bunch arrives at the cavity at a time such that the average accelerating field that it sees in the cavity is zero: the energy of this particle will be unchanged. However, particles ahead or behind this particle will see a non-zero field (on average) and will then either gain or lose energy. The energy change  $\Delta E$  of a particular particle will depend on the distance by which it is either ahead or behind the centre of the bunch, the RF voltage and frequency of the cavity:

$$\Delta E = -eV \sin(kz). \quad (20)$$

Here,  $V$  is the maximum voltage across the cavity (taking into account the time of flight of a particle through the cavity),  $k = \omega/c$  (where  $\omega$  is the RF angular frequency and  $c$  is the speed of light), and  $z$  is the distance of the particle from the centre of the bunch. Note that we use the convention that  $z$  is *positive* for a particle that is *ahead* of the centre of the bunch. In that case, the minus sign in Eq. (20) means that for a bunch of particles moving through the bunch compressor, the RF cavity reduces the energy of particles at the head of the bunch, and increases the energy of particles in the tail (see Fig. 3, bottom).

For convenience, we define the longitudinal phase space variables as  $z$  (the co-ordinate) and  $\delta$ , the energy deviation. The energy deviation  $\delta$  of a particle with energy  $E$  is defined as:

$$\delta = \frac{E - E_0}{E_0}, \quad (21)$$

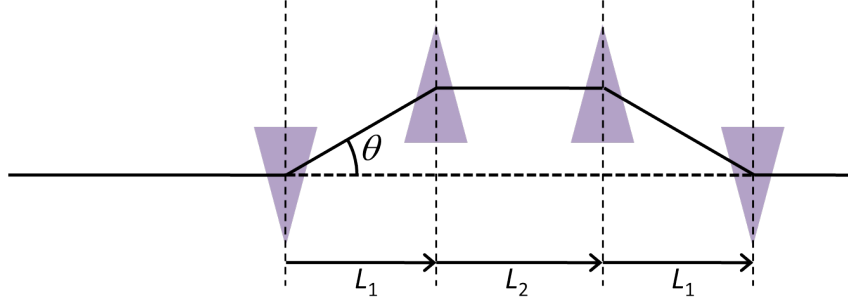


**Fig. 4:** Path of a particle moving through a chicane. Since the bending angle  $\theta$  depends on the energy of a particle, the path length also depends on  $\theta$ : the higher the momentum of a particle, the smaller the angle  $\theta$ , and the shorter the path of the particle through the chicane.

where  $E_0$  is the reference energy for the system (corresponding to the energy of a particle with total momentum  $P_0$ , the reference momentum). If the reference momentum is chosen so that it is close to the “average” momentum of particles in the beam, then  $\delta$  should be a small number (i.e.  $|\delta| \ll 1$ ) for all particles: this has some advantages when expressing nonlinear transfer maps in terms of power series of the dynamical variables. In terms of the variables  $z$  and  $\delta$ , the transfer map for the RF cavity in the bunch compressor is:

$$z_1 = z_0, \quad (22)$$

$$\delta_1 = \delta_0 - \frac{eV}{E_0} \sin(kz_0). \quad (23)$$

Now consider the dynamics in the sequence of four dipoles following the RF cavity: in the example we are considering here, the dipoles form a chicane, so that for a particle with the reference momentum, the trajectory after the exit of the chicane is colinear with the trajectory at the entrance of the chicane. Neglecting synchrotron radiation, the chicane does not change the energy of the particles. However, the path length  $L$  depends on the energy of the particle. If we assume that the bending angle in each dipole is small,  $\theta \ll 1$ , then from Fig. 4 we find that:

$$L = \frac{2L_1}{\cos(\theta)} + L_2. \quad (24)$$

The bending angle is a function of the energy of the particle:

$$\theta(\delta) = \frac{\theta_0}{1 + \delta}. \quad (25)$$

Assuming that the beam is ultrarelativistic (so that we can neglect differences in the speed of particles arising from differences in energy) the change in the co-ordinate  $z$  of a particle after passing through the chicane is the difference between the nominal path length, and the length of the path actually taken by the particle. Hence, the transfer map for the chicane can be written:

$$z_2 = z_1 + 2L_1 \left( \frac{1}{\cos(\theta_0)} - \frac{1}{\cos(\theta(\delta_1))} \right), \quad (26)$$

$$\delta_2 = \delta_1, \quad (27)$$

where  $\theta_0$  is the nominal bending angle of each dipole in the chicane, and  $\theta(\delta)$  is given by (25).

We can now write down the complete transfer map for the bunch compressor by substituting  $z_1$  and  $\delta_1$  from Eqs. (22) and (23) into Eqs. (26) and (27). Expanding the resulting expressions in terms

of the dynamical variables provides the transfer map in the form of a power series. Using the standard notation, we write:

$$z_2 = R_{55}z_0 + R_{56}\delta_0 + T_{555}z_0^2 + T_{556}z_0\delta_0 + T_{566}\delta_0^2 + \dots \quad (28)$$

$$\delta_2 = R_{65}z_0 + R_{66}\delta_0 + T_{655}z_0^2 + T_{656}z_0\delta_0 + T_{666}\delta_0^2 + \dots \quad (29)$$

The procedure that we have described provides expressions for the coefficients in terms of the bunch compressor parameters. In particular, we find for the coefficients of the linear terms:

$$R_{55} = 1 - \frac{eV}{E_0}kL_1 \frac{\theta_0 \sin(2\theta_0)}{\cos^3(\theta_0)}, \quad (30)$$

$$R_{56} = L_1 \frac{\theta_0 \sin(2\theta_0)}{\cos^3(\theta_0)}, \quad (31)$$

$$R_{65} = -\frac{eV}{E_0}k, \quad (32)$$

$$R_{66} = 1, \quad (33)$$

The coefficients of the second-order terms are given by:

$$T_{555} = \left(\frac{eV}{E_0}k\right)^2 L_1 \frac{\theta_0(\cos(\theta_0) - 3) - 2\sin(2\theta_0)}{2\cos^3(\theta_0)}, \quad (34)$$

$$T_{556} = -\frac{eV}{E_0}kL_1 \frac{\theta_0(\cos(\theta_0) - 3) - 2\sin(2\theta_0)}{\cos^3(\theta_0)}, \quad (35)$$

$$T_{566} = L_1 \frac{\theta_0(\cos(\theta_0) - 3) - 2\sin(2\theta_0)}{2\cos^3(\theta_0)}, \quad (36)$$

$$T_{655} = T_{656} = T_{666} = 0. \quad (37)$$

## 4.2 Linear analysis and initial choice of parameters

Having constructed the transfer map, the next step is to determine appropriate values for the parameters of the main components, based on consideration of the linear dynamics. The first consideration is the compression factor that the bunch compressor should achieve. This can be written in terms of the mean square values of the initial and final longitudinal co-ordinates:

$$\frac{\langle z_2^2 \rangle}{\langle z_0^2 \rangle} = \frac{1}{b^2}, \quad (38)$$

where the brackets  $\langle \cdot \rangle$  indicate an average over all particles in the bunch, and  $b$  is the required compression factor. If we assume that the beam at the entrance to the bunch compressor has no initial chirp, so that  $\langle z_0\delta_0 \rangle = 0$ , then taking only the linear terms from Eq. (28) gives:

$$\langle z_2^2 \rangle = R_{55}^2 \langle z_0^2 \rangle + R_{56}^2 \langle \delta_0^2 \rangle = \frac{\langle z_0^2 \rangle}{b^2}. \quad (39)$$

Generally, the beam exiting the bunch compressor should have no energy chirp, so that  $\langle z_2\delta_2 \rangle = 0$ . Using Eqs. (28) and (29) and again keeping only linear terms gives:

$$\langle z_2\delta_2 \rangle = R_{55}R_{65}\langle z_0^2 \rangle + R_{56}\langle \delta_0^2 \rangle = 0. \quad (40)$$

Note that we have used the fact that  $R_{66} = 1$ . A third (and final) constraint comes from the fact that the linear transfer map must be symplectic: this means that the transfer matrix (with elements  $R_{ij}$ ) must have unit determinant:

$$R_{55} - R_{56}R_{65} = 1. \quad (41)$$



**Table 1:** Design specifications for the bunch compressor in the International Linear Collider.

|                           |                                     |        |
|---------------------------|-------------------------------------|--------|
| Initial rms bunch length  | $\sqrt{\langle z_0^2 \rangle}$      | 6 mm   |
| Initial rms energy spread | $\sqrt{\langle \delta_0^2 \rangle}$ | 0.15%  |
| Final rms bunch length    | $\sqrt{\langle z_2^2 \rangle}$      | 0.3 mm |

With given initial bunch length, energy spread, and specified compression factor, Eqs. (39), (40) and (41) can be solved to give values for  $R_{55}$ ,  $R_{56}$  and  $R_{65}$ . The result is:

$$R_{55} = \frac{1}{b^2}, \quad (42)$$

$$R_{56} = \pm \frac{\sqrt{b^2 - 1}}{b^2} \sqrt{\frac{\langle z_0^2 \rangle}{\langle \delta_0^2 \rangle}}, \quad (43)$$

$$R_{65} = \mp \sqrt{b^2 - 1} \sqrt{\frac{\langle \delta_0^2 \rangle}{\langle z_0^2 \rangle}}. \quad (44)$$

As an example, let us consider the parameters for the bunch compressors in the International Linear Collider, given in Table 1. With the given initial bunch length and energy spread, and the specified final bunch length (and also since  $R_{56}$  must be positive in this case), we find that:

$$R_{55} = 0.0025, \quad (45)$$

$$R_{56} = 0.19975 \text{ m}, \quad (46)$$

$$R_{65} = -4.9937 \text{ m}^{-1}. \quad (47)$$

Using these values, we can illustrate the effect of the linearised bunch compressor map on phase space. For clarity and convenience, we use an artificial ‘‘window frame’’ distribution: see Fig. 5. Particles are initially distributed along lines in phase space corresponding to one standard deviation of the nominal distribution. We see that after passing through the bunch compressor, and applying only the linear terms in the transfer map, the rms bunch length is reduced by a factor of 20 as required. The rms energy spread is *increased* by the same factor, but this is unavoidable, because the transfer map is symplectic; this means that phase space areas are conserved under the transformation, i.e. the longitudinal emittance is conserved (as required by Liouville’s theorem).

Based on the values for the coefficients in the transfer map given in (45), (46) and (47) we can select appropriate values for the parameters of the main components in the bunch compressor. These will also be determined by technical considerations and constraints from the overall design of the facility. Such considerations are beyond the scope of this discussion; but it is found that the parameters given in Table 2 are suitable for the case of the International Linear Collider.

### 4.3 Nonlinear analysis and optimisation of parameters

Using the values of the parameters given in Table 2, we can move on to the next step in the design process, which is to evaluate the impact of nonlinear effects. As before, we illustrate the effect of the bunch compressor map on phase space using a ‘‘window frame’’ distribution; this time, however, we can apply the full transfer map expressed in Eqs. (22), (23), (26) and (27). The results are shown in Fig. 6. Although the bunch length has been reduced, there is significant distortion of the distribution: the rms bunch length will be significantly longer than the specification requires. To reduce the distortion, we first need to understand where it comes from, which means looking at the map more closely. Consider a

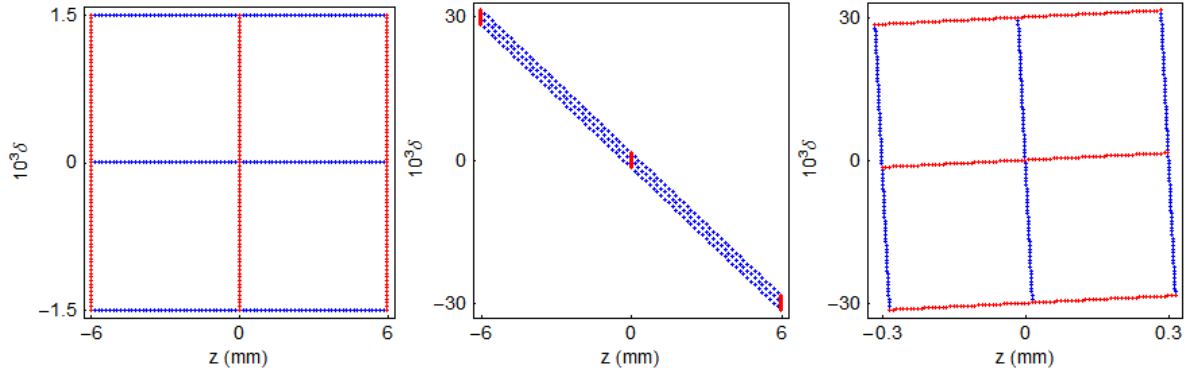


**Fig. 5:** Effect of the linear part of the map for a bunch compressor on particles in longitudinal phase space. Left: initial “window frame” distribution. Middle: distribution after passing through the RF cavity, which imparts a chirp (correlation between energy and longitudinal position) to the bunch. Right: final distribution after exiting the chicane.

**Table 2:** Parameters of components in a bunch compressor designed (on the basis of the linear part of the transfer map) to achieve the specifications given in Table 1.

|                      |            |              |
|----------------------|------------|--------------|
| Beam energy          | $E_0$      | 5.00 GeV     |
| RF frequency         | $f$        | 1.3 GHz      |
| RF voltage           | $V$        | 916 MV       |
| Dipole spacing       | $L_1$      | 36.3 m       |
| Dipole bending angle | $\theta_0$ | $3.00^\circ$ |

particle entering the bunch compressor with initial energy deviation  $\delta_0 = 0$ . From the shape of the final phase space<sup>2</sup>, we see that the final co-ordinate  $z_2$  varies *quadratically* with the initial  $z_0$ :

$$z_2 \propto z_0^2. \quad (48)$$

This suggests that the distortion is dominated by the term in the transfer map with coefficient  $T_{555}$ . To eliminate the distortion, we see from (34) that we would need to choose a bending angle  $\theta_0$  in the chicane that satisfies:

$$\theta_0(\cos(\theta_0) - 3) - 2\sin(\theta_0) = 0. \quad (49)$$

Unfortunately, the only solution to this equation is  $\theta_0 = 0$ , which would eliminate the chicane altogether, and is incompatible with the linear part of the transfer map. To address the problem of the phase space distortion caused by the nonlinearities, we need to introduce an additional degree of freedom.

Understanding the physical origin of the damaging nonlinearity will help us to identify a possible solution. Since the RF cavity has no effect on the longitudinal co-ordinate, the  $T_{555}$  term in the transfer map must come from the chicane: this is confirmed by our observation above, that  $T_{555} = 0$  if  $\theta_0 = 0$ , i.e. if we eliminate the chicane altogether. The physical cause of the nonlinear distortion is the second-order dependence of the change in longitudinal co-ordinate on the energy deviation for a particle passing through a dipole. Unfortunately, this effect is intrinsic to dipole magnets, and cannot be corrected within the magnet itself. However, we can compensate for it if we introduce a second-order dependence of the energy deviation on the longitudinal co-ordinate before the bunch enters the chicane.

<sup>2</sup>Note that points along lines of constant energy deviation in the initial phase space are coloured blue: because of the rotation of phase space, the  $\delta$  axis in the final phase space plot corresponds (approximately) to the  $z$  axis in the initial phase space plot.

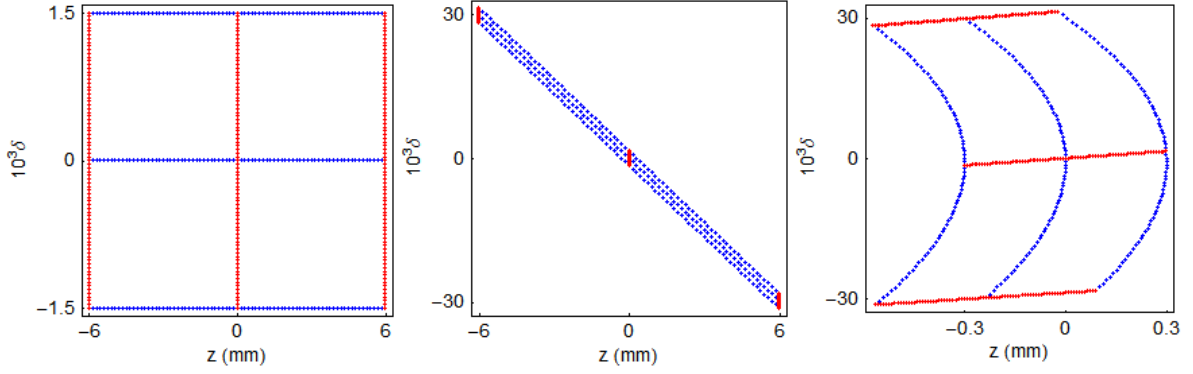


**Fig. 6:** Effect of the full nonlinear map for a bunch compressor on particles in longitudinal phase space. Left: initial “window frame” distribution. Middle: distribution after passing through the RF cavity, which imparts a chirp (correlation between energy and longitudinal position) to the bunch. Right: final distribution after exiting the chicane.

To see how this works, suppose that we write the transformation of the energy deviation in the first part of the bunch compressor as follows:

$$\delta_1 = R_{65}^{(1)} z_0 + T_{655}^{(1)} z_0^2. \quad (50)$$

We use the superscript on  $R_{ij}^{(1)}$  and  $T_{ijk}^{(1)}$  to indicate that the coefficient is for the map for only the first part of the bunch compressor. Then, we write the transformation for the longitudinal co-ordinate in the second part of the bunch compressor:

$$z_2 = R_{56}^{(2)} \delta_1 + T_{566}^{(2)} \delta_1^2. \quad (51)$$

Substituting  $\delta_1$  from (50) into (51), and keeping terms only up to second order, we find:

$$z_2 = R_{56}^{(2)} R_{65}^{(1)} z_0 + R_{56}^{(2)} T_{655}^{(1)} z_0^2 + T_{566}^{(2)} \left( R_{65}^{(1)} \right)^2 z_0^2. \quad (52)$$

In the transfer map we have used so far for the RF cavity in the bunch compressor,  $T_{655}^{(1)} = 0$ : there is then a second-order dependence of  $z_2$  on  $z_0$ , with coefficient  $T_{566}^{(2)} \left( R_{65}^{(1)} \right)^2$ . To eliminate this dependence, we need to modify the transformation in the RF cavity so that:

$$T_{555} = R_{56}^{(2)} T_{655}^{(1)} + T_{566}^{(2)} \left( R_{65}^{(1)} \right)^2 = 0. \quad (53)$$

To achieve this, we simply need to change the phase of the RF cavity, so that a particle at the centre of the bunch sees a non-zero accelerating (or decelerating) field:

$$\delta_{1a} = \delta_0 - \frac{eV}{E_0} \sin(kz_0 + \phi_0). \quad (54)$$

Although this will introduce the terms that we need in the map to correct the nonlinear distortion, it also means that there is an overall change in the bunch energy. The overall change in energy is inconvenient for the description of the dynamics in the chicane: in order to maintain good accuracy in the power series representation of the transfer map, it is desirable for particles in the bunch to be described by small values of the energy deviation, with mean of zero. To ensure that this is the case, we change the reference energy from  $E_0$  to  $E_0 - eV \sin(\phi_0)$ . This change in reference energy will restore the mean energy deviation

of the bunch to zero; but we also need to take into account, from Eq. (21), that when we change the reference energy from  $E_0$  to a new value  $E'_0$ , the energy deviation changes from  $\delta$  to  $\delta'$ :

$$\delta' = \left( \delta - \frac{\Delta E_0}{E_0} \right) \frac{E_0}{E'_0}, \quad (55)$$

where  $\Delta E_0 = E'_0 - E_0$ . This scaling of the momentum deviation, with no associated change in the longitudinal co-ordinate, is a non-symplectic transformation, and leads to a change in the longitudinal emittance. A similar effect occurs in the transverse degrees of freedom: when associated with acceleration in a linac, it leads to a reduction of the emittances in all three planes, and is known as *adiabatic damping*. In the present case of the bunch compressor, the result is that the full transformation in the RF cavity is now:

$$z_1 = z_0, \quad (56)$$

$$\delta_1 = \left( \delta_0 - \frac{eV}{E_0} (\sin(kz_0 + \phi_0) - \sin(\phi_0)) \right) \left( 1 - \frac{eV}{E_0} \sin(\phi_0) \right)^{-1}. \quad (57)$$

Expanding to second order in  $z_0$ , this gives:

$$\delta_1 = \left( 1 - \frac{eV}{E_0} \sin(\phi_0) \right)^{-1} \left( \delta_0 - \frac{eV}{E_0} \cos(\phi_0) kz_0 + \frac{eV}{2E_0} \sin(\phi_0) k^2 z_0^2 + \dots \right) \quad (58)$$

Hence:

$$T_{655}^{(1)} = \frac{eV}{2E_0} \sin(\phi_0) k^2. \quad (59)$$

A non-zero value of  $\phi_0$  leads to a non-zero value for  $T_{655}^{(1)}$ , and allows us to satisfy the requirement expressed in Eq. (53), to correct the nonlinear distortion arising from  $T_{566}^{(2)}$ . The other constraints that we need to satisfy are, as before, the specified reduction in bunch length, Eq. (39):

$$R_{55}^2 + \frac{\langle \delta_0^2 \rangle}{\langle z_0^2 \rangle} R_{56}^2 = \frac{1}{b^2}, \quad (60)$$

and the requirement for zero final energy chirp, Eq. (40):

$$R_{55} R_{65} + \frac{\langle \delta_0^2 \rangle}{\langle z_0^2 \rangle} R_{56} R_{66} = 0. \quad (61)$$

Note that the expressions for the coefficients  $R_{ij}$  need to be re-calculated for the case  $\phi_0 \neq 0$ : in particular  $R_{66}$  is no longer equal to 1. Also, the constraint expressed in Eq. (40) no longer applies, because of the (non-symplectic) rescaling of the reference energy that we have applied following the RF cavity.

We therefore have three constraints, Eq. (53), (60) and (61). Assuming fixed RF frequency and dipole spacing<sup>3</sup>, we can satisfy the constraints by adjusting the values of the RF voltage  $V$ , the RF phase  $\phi_0$ , and the dipole bending angle  $\theta_0$ . Given the complicated, nonlinear nature of the constraint equations, the parameter optimisation is best done numerically. Suitable values for the parameters are shown in Table 3.

As before, we illustrate the effect of the bunch compressor on phase space using a “window frame” distribution. But now we use the parameters given in Table 3 to aim to compress the bunch length by a factor 20 while minimising the second-order distortion: the results are shown in Fig. 7. We see that the nonlinear distortion is greatly reduced: the remaining distortion now appears to be dominated by third-order terms, and appears to be small enough that it should not significantly affect the performance of the machine.

<sup>3</sup>The RF frequency and dipole spacing are fixed at time of machine construction; the RF voltage, RF phase, and dipole bending angle are readily adjusted during operation.

**Table 3:** Parameters of components in a bunch compressor designed to achieve the specifications given in Table 1, and taking into account the effects of nonlinear dynamics. The parameter values are to be compared with those in Table 2, which were determined on the basis only of the linear dynamics.

|                      |            |               |
|----------------------|------------|---------------|
| Initial beam energy  | $E_0$      | 5.00 GeV      |
| Final beam energy    | $E'_0$     | 4.43 GeV      |
| RF frequency         | $f$        | 1.3 GHz       |
| RF voltage           | $V$        | 1079 MV       |
| RF phase             | $\phi_0$   | $31.86^\circ$ |
| Dipole spacing       | $L_1$      | 36.3 m        |
| Dipole bending angle | $\theta_0$ | $2.83^\circ$  |

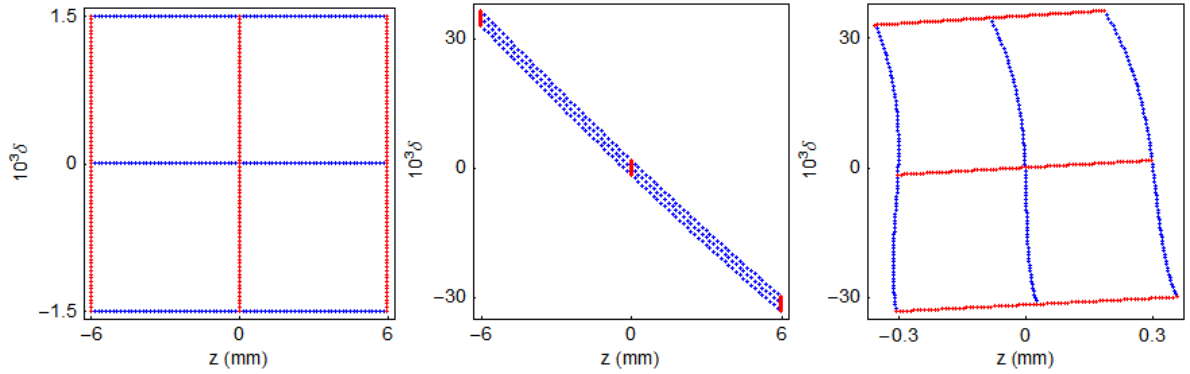


**Fig. 7:** Effect of the full nonlinear map for a bunch compressor on particles in longitudinal phase space, with parameters adjusted to compensate for the nonlinear distortion seen in Fig. 6. Left: initial “window frame” distribution. Middle: distribution after passing through the RF cavity, which imparts a chirp (correlation between energy and longitudinal position) to the bunch. Right: final distribution after exiting the chicane.

#### 4.4 Summary: lessons from analysis of the bunch compressor

The analysis of the bunch compressor presented in this section highlights some important aspects of nonlinear dynamics in accelerators. First, we see that nonlinear effects can limit the performance of an accelerator system. Sometimes the effects are small enough that they can be ignored; however, in many cases, a system designed without taking account of nonlinearities will not achieve the specified performance. Secondly, a careful analysis can lead to an understanding of the nonlinear behaviour of a system, including the origin of the nonlinearities. Based on this analysis, it may be possible to find a means of compensating any adverse effects.

### 5 Nonlinear dynamics in a storage ring

In this section, we consider some of the phenomena associated with nonlinear dynamics in periodic beamlines, using a storage ring as an example. We will explain the significance of *symplectic maps*, and describe some of the challenges in constructing and applying symplectic maps. Finally, we will outline some of the analysis methods that can be used to characterise nonlinear beam dynamics in periodic beamlines.

In the discussion of a bunch compressor in the previous section of these notes, we focused on the longitudinal dynamics. For the case of a storage ring, we shall be concerned with the transverse dynamics. Nonlinear effects can impact both longitudinal and transverse motion, and in many cases it

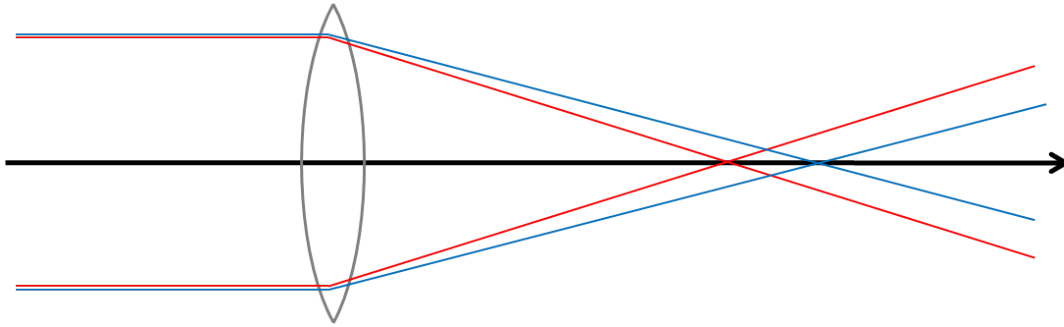


**Fig. 8:** Chromaticity in a quadrupole magnet. The beam rigidity increases with energy, leading to an increase in the focal length of a quadrupole with particle energy.

may be necessary to consider both. This is indeed the case in many storage rings; but for simplicity, we shall restrict the discussion to the transverse dynamics.

We shall make the following assumptions:

- the storage ring is constructed from some number of identical cells consisting of dipoles, quadrupoles and sextupoles;
- the phase advance per cell can be tuned from close to zero, up to about  $0.5 \times 2\pi$ .
- there is a single sextupole per cell, located at a point where the horizontal beta function is 1 m, and the alpha function is zero.

Usually, storage rings will contain (at least) two sextupoles per cell, to correct horizontal and vertical chromaticity. Again for the sake of simplicity, we will use only one sextupole per cell.

### 5.1 Correction of chromaticity using sextupole magnets

Sextupoles are needed in a storage ring to compensate for the fact that quadrupoles have lower focusing strength for particles of higher energy (see Fig. 8): this is characterised by the chromaticity, which is defined as the change in particle tune in a storage ring with respect to energy deviation. Chromaticity often has undesirable consequences. For example, if particles with sufficiently large energy deviation (by virtue of the natural energy spread of the beam) have betatron tunes close to integer or half-integer values, then the motion of these particles can become unstable, leading to loss of the particles from the storage ring.

A sextupole can be regarded as a quadrupole with focusing strength that increases with horizontal (transverse) distance from the axis of the magnet. If sextupoles are located where there is non-zero dispersion, they can be used to control the chromaticity in a storage ring. The dispersion describes the change in position of the closed orbit with respect to changes in energy deviation: particles with higher energy deviation will then pass through the sextupole further from the axis of the magnet (see Fig. 9), and hence receive additional focusing or defocusing. By adjusting the strength of the sextupole (depending on the size of the dispersion), it is possible to compensate the natural chromaticity arising from the variation of the focal lengths of the quadrupoles with particle energy.

The chromaticity of a storage ring, and hence the strengths of the sextupoles needed to correct the chromaticity, will normally be a function of the phase advance per cell. However, to investigate and illustrate the nonlinear effects of the sextupoles, we shall assume that we keep the strength  $k_2 L$  of the sextupoles in our simple storage ring fixed when we change the phase advance. Although this means that the chromaticity will in general be non-zero, since we shall be looking only at the motion of particles with zero energy deviation, the chromaticity will play no real role. The effects of the sextupoles in this case are

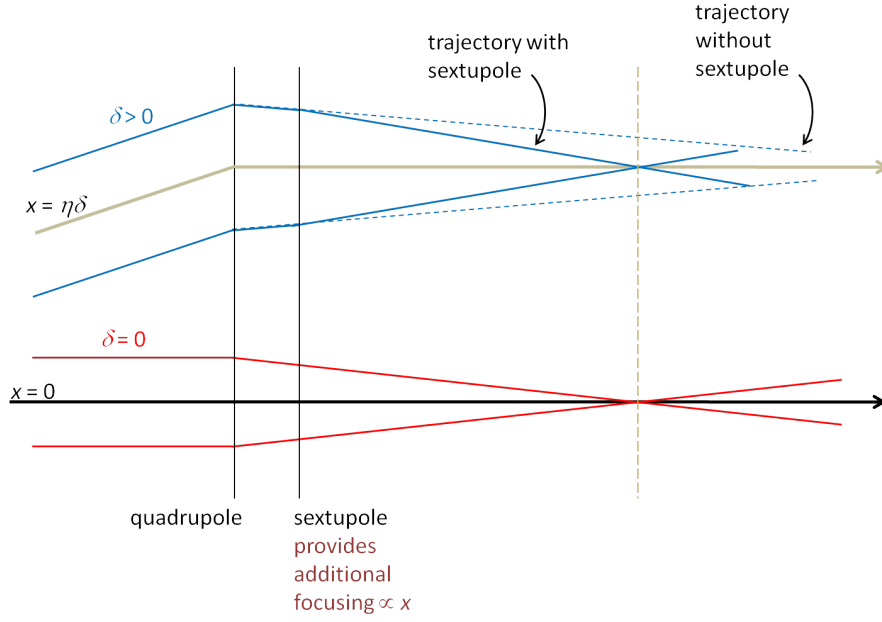


**Fig. 9:** Correction of chromaticity in a quadrupole magnet, using a sextupole at a location with non-zero dispersion.

sometimes called the *geometric* effects, to distinguish them from the chromatic effects. The geometric effects of sextupoles can have significant adverse impact on the stability of the motion of particles in a storage ring. Particularly for low-emittance electron storage rings, for example in third-generation synchrotron light sources, it is an important task at the design stage to optimize the chromatic effects of the sextupoles while minimising the geometric effects, in order to achieve a good beam lifetime.

In our simple storage ring, we can assume that the map from one sextupole to the next is linear, and corresponds to a rotation in phase space through an angle equal to the phase advance:

$$\begin{pmatrix} x \\ p_x \end{pmatrix} \mapsto \begin{pmatrix} \cos(\mu_x) & \sin(\mu_x) \\ -\sin(\mu_x) & \cos(\mu_x) \end{pmatrix} \begin{pmatrix} x \\ p_x \end{pmatrix}. \quad (62)$$

Note that we use the symbol  $\mapsto$  to mean “transforms to”: this avoids the need to use subscripts to indicate initial and final values of the phase space variables (as in, for example,  $x_0$  and  $x_1$ ). Again to keep things simple, we shall consider only horizontal motion, and assume that the vertical co-ordinate  $y = 0$ .

The change in the horizontal momentum of a particle moving through the sextupole is found by integrating the Lorentz force over the length  $L$  of the sextupole:

$$\Delta p_x = - \int_0^L \frac{B_y}{B\rho} ds. \quad (63)$$

The sextupole strength  $k_2$  is defined by:

$$k_2 = \frac{1}{B\rho} \frac{\partial^2 B_y}{\partial x^2}, \quad (64)$$

where  $B\rho$  is the beam rigidity. For a pure sextupole field, in the case that the vertical co-ordinate  $y = 0$ , the vertical component of the magnetic field is given by:

$$\frac{B_y}{B\rho} = \frac{1}{2} k_2 x^2. \quad (65)$$

If the sextupole is short (compared to the betatron wavelength), then we can neglect the small change in the co-ordinate  $x$  as the particle moves through the sextupole, in which case:

$$\Delta p_x \approx -\frac{1}{2}k_2 L x^2. \quad (66)$$

Hence, the transfer map for a particle moving through a short sextupole can be represented by a “kick” in the horizontal momentum:

$$x \mapsto x, \quad (67)$$

$$p_x \mapsto p_x - \frac{1}{2}k_2 L x^2. \quad (68)$$

## 5.2 Effects of sextupoles in a storage ring: dependence on phase advance

To illustrate the effect of the sextupole in our storage ring, let us choose a fixed value  $k_2 L = -600 \text{ m}^{-2}$  for the strength of the sextupole, and look at the effects of the maps for different phase advances. As mentioned above, we shall only consider the case that the particles have zero energy deviation. For a given value of the phase advance, we construct a *phase space portrait* by plotting the values of the dynamical variables after repeated application of the transfer map (equation (62), followed by (67) and (68)) for a range of initial conditions. The phase space portraits for the simple storage ring with a range of phase advances from  $0.2 \times 2\pi$  to  $0.5 \times 2\pi$  are shown in Fig. 10.

There are some interesting features in these phase space portraits to which it is worth drawing attention:

- For small amplitudes (small  $x$  and  $p_x$ ), particles trace out closed loops around the origin: this is what we expect for a purely linear map.
- As the amplitude is increased, “islands” appear in the phase space, with the number of islands related to the phase advance: the phase advance (for the linear map) is often close to  $m/p$  where  $m$  is an integer and  $p$  is the number of islands.
- Sometimes, a larger number of islands appears at larger amplitude.
- Usually, there is a closed curve that divides a region of stable motion from a region of unstable motion. Outside that curve, the amplitude of particles increases without limit as the map is repeatedly applied, i.e. the motion is unstable.
- The area of the stable region depends strongly on the phase advance: for a phase advance close to  $2\pi/3$ , it appears that the stable region almost vanishes altogether.
- As the phase advance is increased towards  $\pi$ , the stable area becomes large, and distortions from the linear ellipse become less evident.

An important observation is that the effect of the sextupole in the periodic cell depends strongly on the phase advance across the cell. We can start to understand the significance of the phase advance by considering two special cases: first, the case when the phase advance is equal to an integer times  $2\pi$ ; and second, when the phase advance is equal to a half integer times  $2\pi$ . In the first case, when the phase advance is an integer, the linear part of the map is just the identity:

$$x \mapsto x, \quad (69)$$

$$p_x \mapsto p_x. \quad (70)$$

So the combined effect of the linear map and the sextupole kick is:

$$x \mapsto x, \quad (71)$$

$$p_x \mapsto p_x - \frac{1}{2}k_2 L x^2. \quad (72)$$



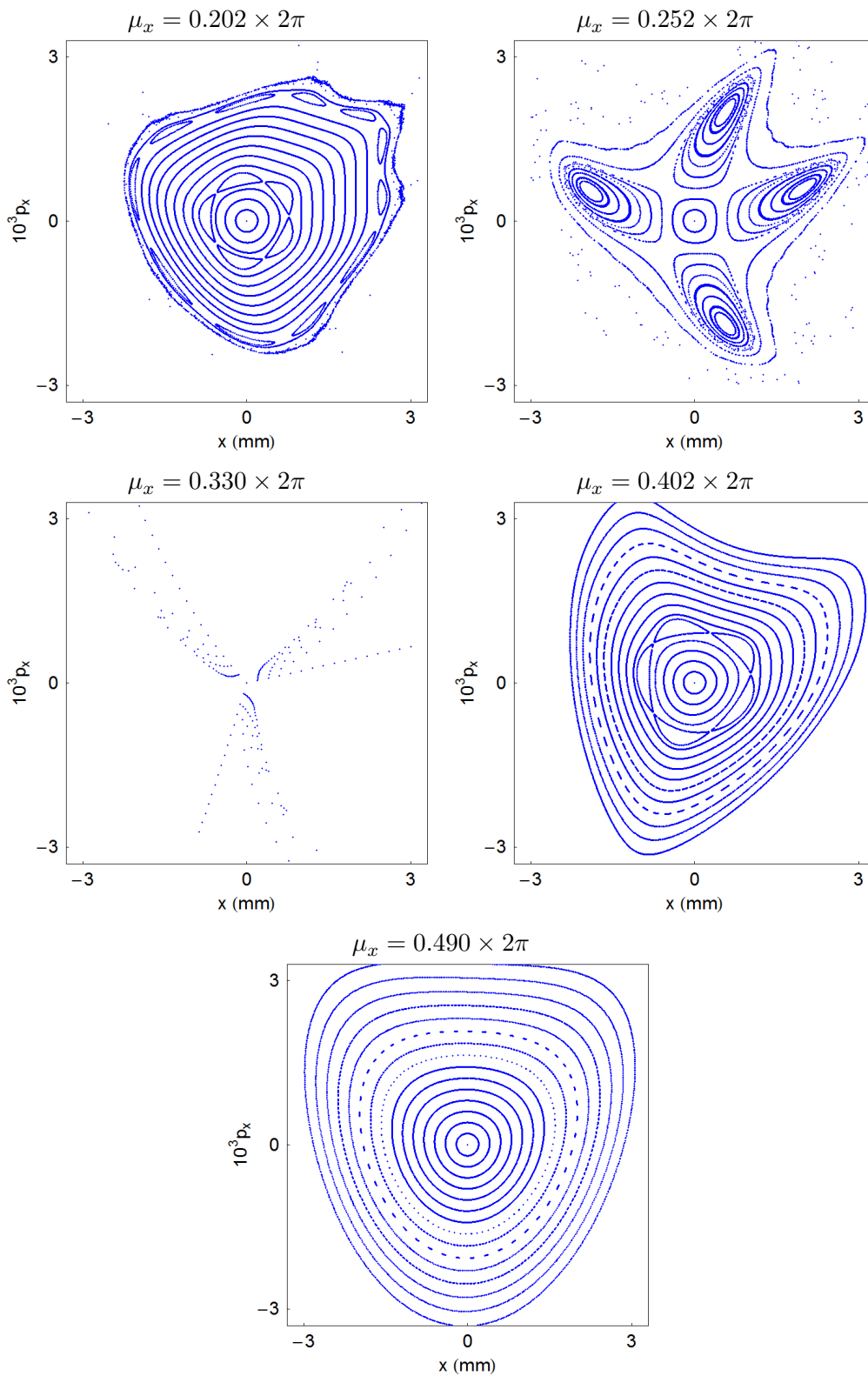


**Fig. 10:** Phase space portraits for a simple storage ring, tuned to various different values of the phase advance per cell, and containing (in addition to the quadrupoles) a single sextupole per cell.

Clearly, for  $x \neq 0$ , the horizontal momentum will increase without limit. There are no stable regions of phase space, apart from the line  $x = 0$ .

Now consider what happens in the second case, when the phase advance over one cell is a half integer times  $2\pi$ , so the linear part of the map is just a rotation by  $\pi$ . If a particle starts at the entrance of a sextupole with  $x = x_0$  and  $p_x = p_{x0}$ , then at the exit of that sextupole (using the subscript notation to indicate initial and final values of the variables):

$$x_1 = x_0, \quad (73)$$

$$p_{x1} = p_{x0} - \frac{1}{2}k_2Lx_0^2. \quad (74)$$

Then, after passing to the entrance of the next sextupole, the phase space variables will be:

$$x_2 = -x_1 = -x_0, \quad (75)$$

$$p_{x2} = -p_{x1} = -p_{x0} + \frac{1}{2}k_2Lx_0^2. \quad (76)$$

Finally, on passing through the second sextupole:

$$x_3 = x_2 = -x_0, \quad (77)$$

$$p_{x3} = p_{x2} - \frac{1}{2}k_2Lx_2^2 = -p_{x0}. \quad (78)$$

In other words, the momentum kicks from the two sextupoles in successive cells cancel each other exactly, and the resulting map is a purely linear phase space rotation by  $\pi$ . In this situation, we expect the motion to be stable (and periodic), regardless of the amplitude.

### 5.3 Resonances

The important conclusion is that the effect of sextupole “kicks” depends on the phase advance between the sextupoles. This is similar to the case of perturbations arising from dipole and quadrupole errors in a storage ring. In the case of dipole errors, the kicks add up if the phase advance is an integer, and cancel if the phase advance is a half integer, see Fig. 11. In the case of quadrupole errors, the kicks add up if the phase advance is a half integer. In general, there are certain values of the phase advance, termed *resonances*, at which small perturbations to the motion applied in each periodic section combine to cause particle motion to be unstable. If we include vertical as well as horizontal motion, then we find that resonances occur when the tunes satisfy:

$$m_x\nu_x + m_y\nu_y = \ell, \quad (79)$$

where  $m_x, m_y$  and  $\ell$  are integers. The *order* of the resonance is  $|m_x| + |m_y|$ : the case  $|m_x| + |m_y| = 1$  is an integer resonance;  $|m_x| + |m_y| = 2$  is a 2<sup>nd</sup> order resonance (or half-integer resonance if  $m_x = 0$  or  $m_y = 0$ ), and so on. Resonances can be illustrated on a resonance diagram, see Fig. 12. The effect of a resonance depends on the order of the resonance, and the presence of components or perturbations that can “drive” the resonance. Although it is tempting to associate resonances of a particular order with corresponding multipoles, in reality the situation is rather complicated: it turns out that sextupoles (and other higher-order multipoles) can drive resonances of many different orders depending on the exact situation.

Resonances are associated with unstable motion for particles in storage rings. However, the number of resonance lines in tune space is infinite: any point in tune space will be close to a resonance of some order. This raises two questions: first, how do we know what the real effect of any given resonance line will be? Second, how can we design a storage ring to minimise the adverse effects of resonances?

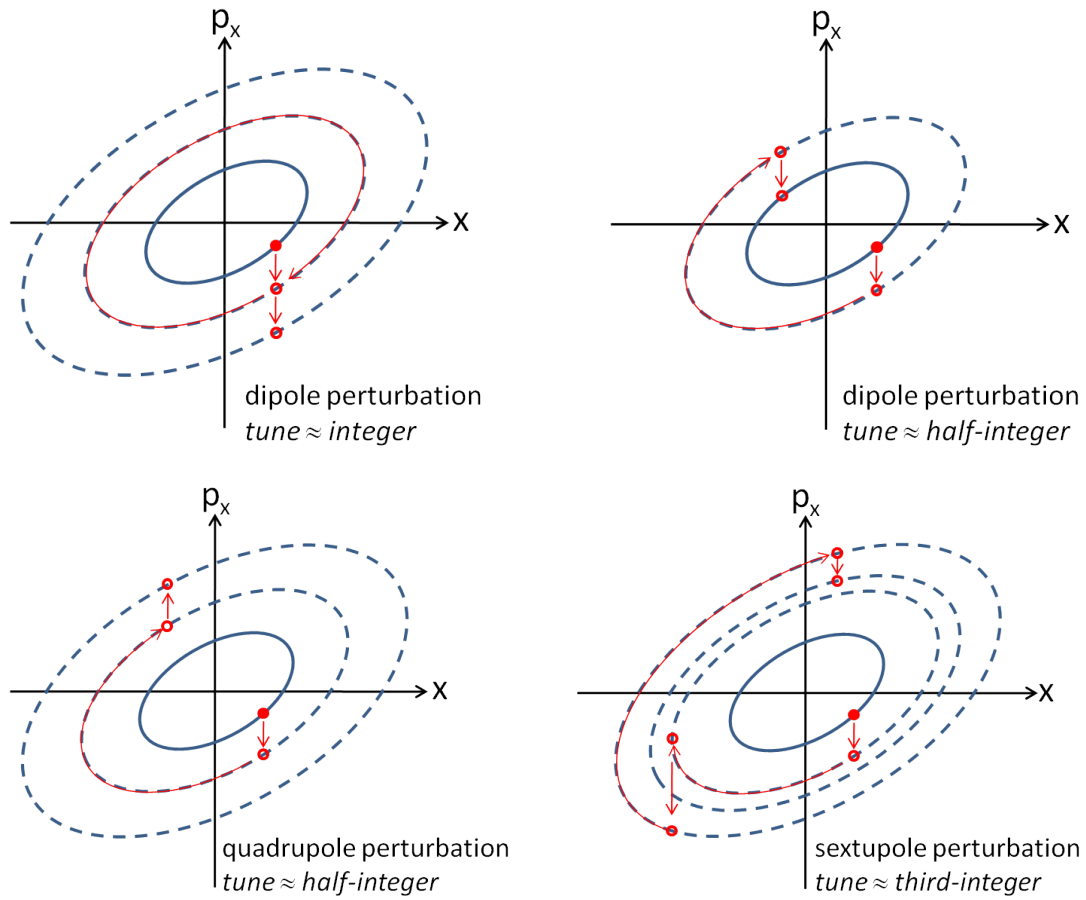


**Fig. 11:** Integer (top) and half-integer (bottom) resonances driven by dipole and quadrupole perturbations (respectively) in a storage ring.

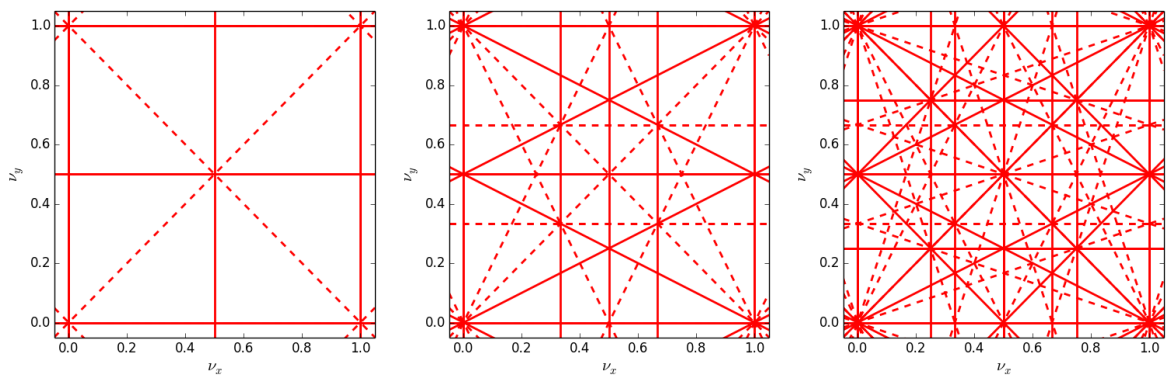


**Fig. 12:** Resonances in a storage ring illustrated in tune space. The horizontal axis corresponds to the fractional part of the horizontal tune, and the vertical axis corresponds to the fractional part of the vertical tune. The lines show where the values of the tunes satisfy the resonance condition  $m_x \nu_x + m_y \nu_y = \ell$ , for integers  $m_x$ ,  $m_y$  and  $\ell$ . Resonances are shown up to 2<sup>nd</sup> order (left), 3<sup>rd</sup> order (middle) and 4<sup>th</sup> order (right). Solid lines indicate resonances associated with normal multipole components and dashed lines indicate resonances associated with skew multipole components of the magnetic field expansion [3].

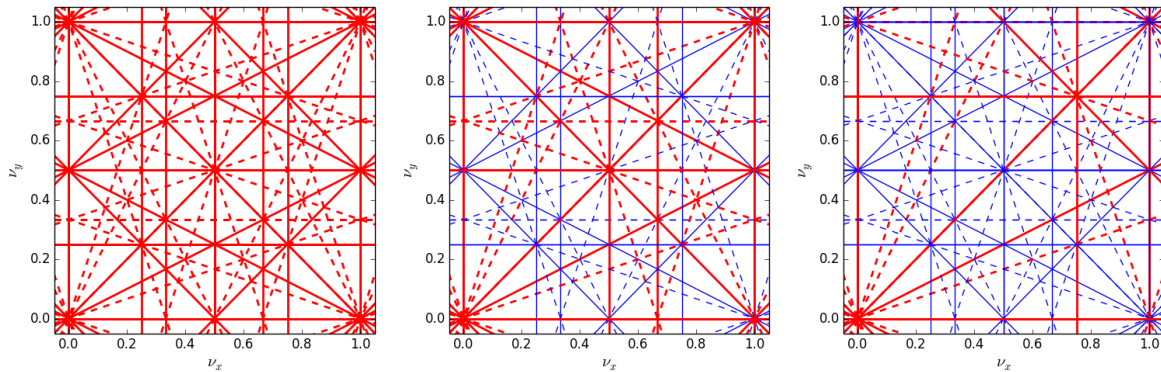


**Fig. 13:** Resonances up to 4<sup>th</sup> order in a storage ring with periodicity  $P = 1$  (left),  $P = 2$  (middle) and  $P = 3$  (right). Red lines indicate systematic resonances, while the blue lines show the non-systematic resonances which (to first order) are suppressed by the lattice symmetry. Solid lines indicate resonances associated with normal multipole components and dashed lines indicate resonances associated with skew multipole components of the magnetic field expansion [3].

From the discussion above, we have seen that for certain phase advances the kicks from sextupole magnetic fields can be cancelled in successive passages of a particle through a periodic cell. It turns out that certain resonances can be suppressed by constructing a lattice with some periodicity  $P$ , i.e. building a machine from  $P$  identical cells. In that case, a resonance corresponding to a particular value of  $\ell$  in the resonance condition Eq. (79) is suppressed by the lattice symmetry (to first order) if  $\ell/P$  is not an integer. This means that the kicks from the magnetic fields in consecutive cells cancel out over one turn, and the lattice does not “drive” the resonance: the resonance is called *non-systematic*. Of course, this is (strictly speaking) only true if the lattice is perfectly periodic, and any variation, for example from random errors in the strengths of the magnets, can break the symmetry and drive nominally non-systematic resonances.

If  $\ell/P$  (for a given resonance) is an integer, the resonance will be *systematic*. In this case, the kicks from consecutive cells of the lattice add up coherently. Figure 13 shows a comparison of the resonance diagram for different lattice periodicities  $P$ . If the “ideal” symmetry of a lattice is broken by random errors or other effects, then the periodicity is effectively reduced to  $P = 1$ , so  $\ell/P$  is an integer for any integer  $\ell$ : all resonances in that case are systematic.

One way to understand systematic resonances is to consider the “tunes” of individual cells in a periodic lattice (i.e. the phase advances per cell, divided by  $2\pi$ ): if the periodicity is  $P$ , then each periodic cell has tunes  $\nu_x/P$  and  $\nu_y/P$ . It follows from the resonance condition Eq. (79) that:

$$m_x \frac{\nu_x}{P} + m_y \frac{\nu_y}{P} = \frac{\ell}{P}, \quad (80)$$

and hence if  $\ell/P$  is an integer, the resonance condition is satisfied for each individual cell, as well as for the full lattice.

A powerful technique to minimise the impact of resonances on the beam is therefore to design storage rings and synchrotrons (or the arcs of colliders) with a high periodicity. A good example illustrating the suppression of resonances through lattice periodicity was demonstrated at the Advanced Light Source (ALS) at Lawrence Berkeley National Laboratory (LBNL). Figure 14 shows the beam loss rate measured in the ALS for a range of different horizontal tunes in two machine configurations [4]. In the first configuration, with uncorrected linear machine optics, the  $\beta$ -beating reached approximately 30%. In this configuration, strong losses were observed close to the horizontal 3<sup>rd</sup> order resonance  $3\nu_x = 43$  even though this is a non-systematic resonance for the ideal ALS lattice, which has periodicity  $P = 12$  ( $\ell/P = 43/12$  is not an integer). In the second configuration, following correction of the linear optics (as

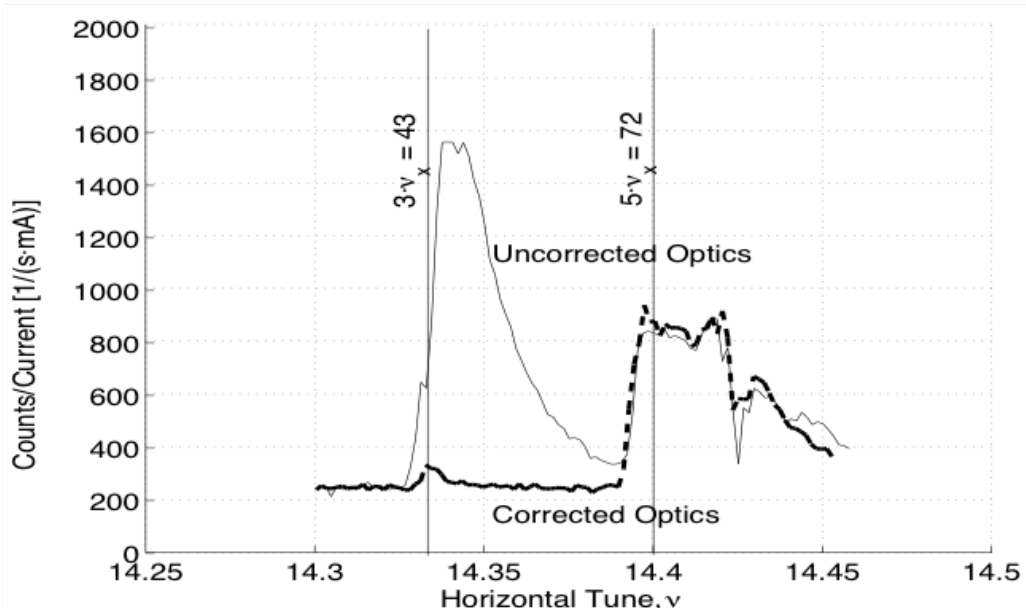


**Fig. 14:** Horizontal tune scans before (thin, solid line) and after (thick, dashed line) optics correction. In the uncorrected optics, the  $\beta$ -beat is of order 30%; following correction, this is reduced to 1%. The vertical tune is kept constant at 8.15. The plot shows the count rate measured in a gamma-ray detector (indicating losses of particles from the beam) divided by beam current [4].

is done in routine machine operation), the  $\beta$ -beating was significantly reduced, to below the 1% level. In this configuration, the beam showed only a very weak sensitivity to the resonance. Thus, by restoring the machine periodicity  $P = 12$  of the ALS by correcting the  $\beta$ -beating, the  $3\nu_x = 43$  resonance was almost completely suppressed. It is also interesting to take a closer look at the loss rates observed close to the  $5\nu_x = 72$  resonance, also seen in Fig. 14. The level of losses at this resonance is practically the same for both machine configurations, i.e. without optics correction and with optics correction. The similarity in the losses in both configurations is explained by the fact that  $5\nu_x = 72$  is a systematic resonance ( $\ell/P = 72/12 = 6$  is an integer) and therefore there is no suppression of the resonance after restoring the lattice periodicity.

Another way of demonstrating the suppression of the 3<sup>rd</sup> order resonance through the lattice periodicity was also demonstrated at the ALS, during the same experiment [4]. Synchrotron radiation images were recorded for a machine working point close to the 3<sup>rd</sup> order resonance  $3\nu_x = 43$  as shown in Fig. 15 (top). Before optics correction, the image showed the beam “split” into several spots; after optics correction (restoring the periodicity of the lattice) only a single beam spot is observed. This observation can be understood from the phase space topology obtained from a machine model for the two configurations, as shown in Fig. 15 (bottom). For the uncorrected optics, the resonance distorts the phase space and creates resonant “islands” in phase space. The islands are populated by electrons in the beam, so that each island, in addition to the central part of the beam, acts as a source of synchrotron radiation. The separation between the islands in phase space (projected onto the co-ordinate axes) is visible on the synchrotron light monitor. This phase space structure does not exist for the machine with restored periodicity, as the resonance is suppressed. The phase space looks highly linear and only one beam spot is observed.

Another example of resonance excitation in operational conditions is provided by the Super Proton Synchrotron (SPS) at CERN [25, 26]. Figure 16 shows a measurement of the beam loss rate for a two-dimensional tune scan. Even though the SPS has a design lattice periodicity of  $P = 6$ , which

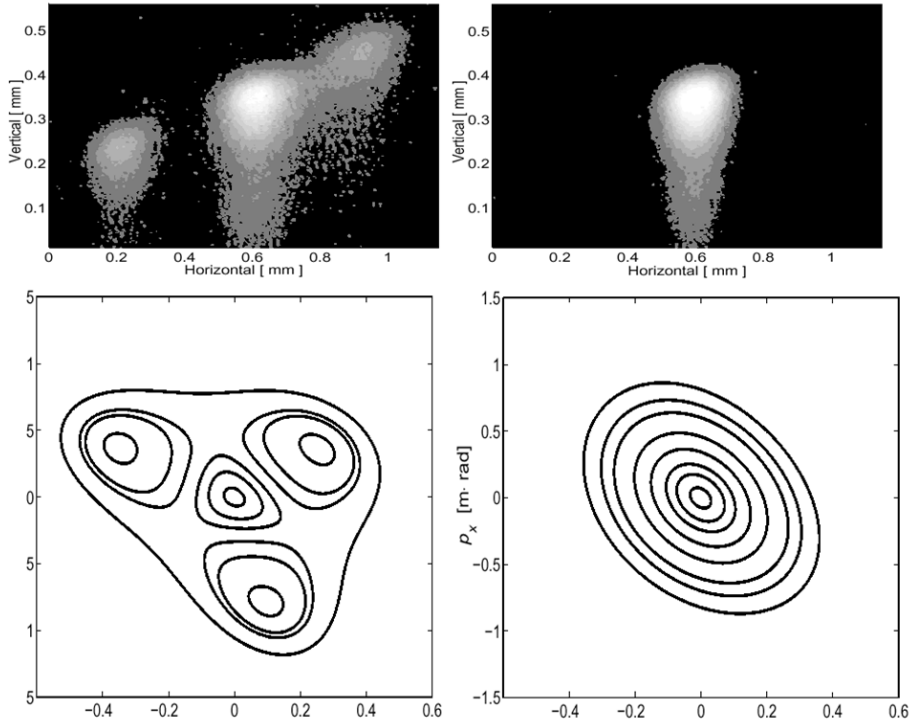


**Fig. 15:** The upper images are taken from a synchrotron radiation monitor in the Advanced Light Source at Lawrence Berkeley National Laboratory, with the lattice tuned near the  $3\nu_x$  resonance. The image on the left was taken before correction of the optics to reduce  $\beta$ -beating; the image on the right was taken after optics correction. (Note that the vertical asymmetry is the result of some distortion in the light optics.) The lower plots show, for comparison, corresponding horizontal phase space topologies obtained from particle tracking in a machine model [4].

suppresses most of the  $3^{\text{rd}}$  order resonances (i.e. they are non-systematic), residual beam loss is observed on practically all  $3^{\text{rd}}$  order normal resonances (solid lines). These resonances are observed to be excited because of perturbations of the linear optics at the level of typically around 10%  $\beta$ -beating, which in the case of the SPS cannot be corrected as it has no individually powered quadrupole magnets. This situation is not unusual for hadron machines (such as the synchrotrons of the injector chain of the LHC, the Large Hadron Collider at CERN). If necessary, resonances are compensated by dedicated multipole corrector magnets.

The optimisation of the nonlinear beam dynamics and thus the machine performance usually requires use of a combination of tools, such as numerical integration of particle motion (tracking) as well as analytical tools, as we will discuss in the remaining parts of these notes.

## 5.4 Symplecticity

For any detailed analysis of nonlinear dynamics in an accelerator, we need a convenient way to represent nonlinear transfer maps. In our analysis of a bunch compressor in section 4, we represented the transfer maps for the RF cavity and the chicane as power series in the dynamical variables. For example, the longitudinal transfer map for a chicane can be written as

$$z_1 = z_0 + 2L_1 \left( \frac{1}{\cos(\theta_0)} - \frac{1}{\cos(\theta)} \right), \quad (81)$$

$$\delta_1 = \delta_0, \quad (82)$$

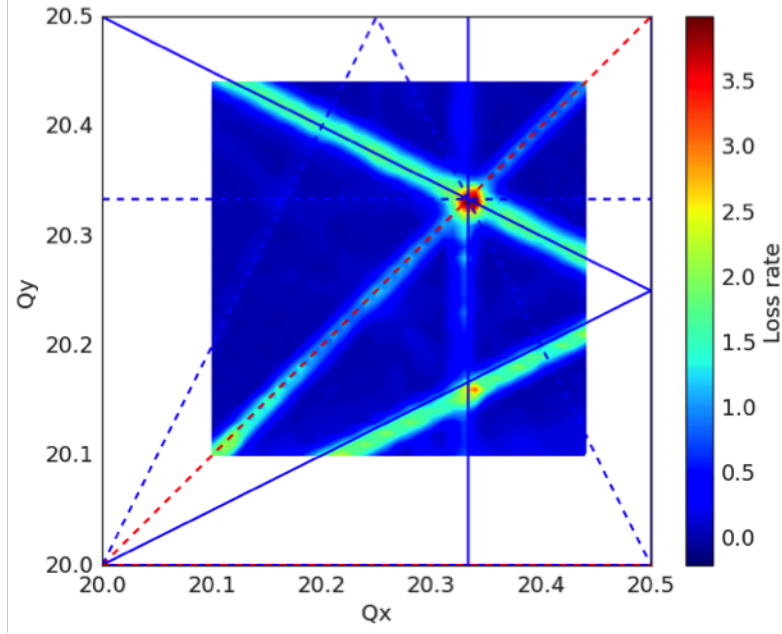


**Fig. 16:** Measurement of the beam loss rate for two-dimensional tune scan at the CERN SPS. The loss rate (in arbitrary units) is indicated by the color scale. The lines indicate resonances up to 3<sup>rd</sup> order, where systematic resonances are indicated in red and non-systematic resonances in blue. Solid lines correspond to normal resonances, dashed lines to skew resonances. The beam shows losses at all the non-systematic normal 3<sup>rd</sup> order resonances, because of linear optics distortions ( $\beta$ -beating).

where

$$\theta = \frac{\theta_0}{1 + \delta_0}. \quad (83)$$

Expanding the map for a chicane as a power series gives

$$z_1 = z_0 + R_{56}\delta_0 + T_{566}\delta_0^2 + U_{5666}\delta_0^3 + \dots \quad (84)$$

$$\delta_1 = \delta_0, \quad (85)$$

where the coefficients  $R_{56}$ ,  $T_{566}$ ,  $U_{5666}$  etc. are all functions of the chicane parameters  $L_1$  and  $\theta_0$ . Power series provide a convenient way of systematically representing transfer maps for beamline components, or sections of beamline. However, the drawback is that in general, transfer maps can only be represented exactly by series with an infinite number of terms. In practice, we have to truncate a power series map at some order, and the consequence is that we can then lose certain desirable properties of the map: in particular, a truncated map will not usually be *symplectic*.

Mathematically, a transfer map is symplectic if it satisfies the condition:

$$J^T S J = S, \quad (86)$$

where  $J$  is the Jacobian of the map, and  $S$  is the antisymmetric matrix with block diagonals:

$$S_2 = \begin{pmatrix} 0 & 1 \\ -1 & 0 \end{pmatrix}. \quad (87)$$

The Jacobian of the map is a matrix with elements  $J_{mn}$  given by:

$$J_{mn} = \frac{\partial x_{m,f}}{\partial x_{n,i}}, \quad (88)$$

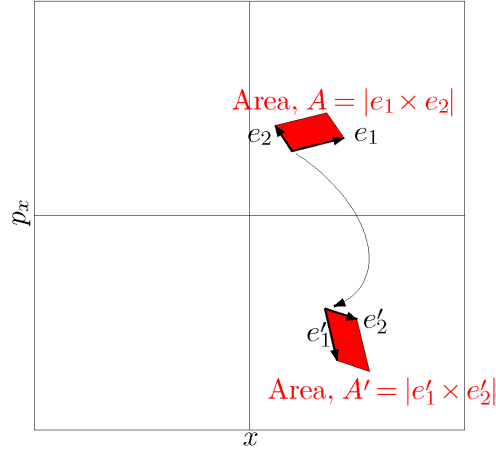


**Fig. 17:** Symplectic transformations conserve the area of elements of phase space.

where  $x_{n,i}$  is the  $n^{\text{th}}$  component of the initial phase space vector  $(x, p_x, y, p_y, z, \delta)$  and  $x_{m,f}$  is the  $m^{\text{th}}$  component of the final phase space vector. For a linear map, the elements of the Jacobian will be constants (i.e. independent of the phase space variables). For nonlinear maps, the elements of the Jacobian will depend on the phase space variables, but if the map is symplectic, then it will still satisfy the condition (88). Physically, a symplectic transfer map conserves phase space volumes when the map is applied. This is Liouville's theorem, illustrated in Fig. 17, and is a property of charged particles moving in electromagnetic fields, in the absence of radiation and certain collective effects.

The effect of losing symplecticity (for example, in the truncation of a power-series map to finite order) becomes apparent if we compare phase space portraits constructed using symplectic and non-symplectic transfer maps: an example is shown in Fig. 18. There are a number of clear differences between the phase space portraits constructed using symplectic and non-symplectic maps. Significantly, the closed loops visible in the “islands” in the symplectic case appear blurred when the non-symplectic map is used. This is an indication that conserved quantities (constraining particle motion in the physical system) are maintained by the symplectic map, but not by the non-symplectic map. This can have some important consequences for the conclusions drawn from an analysis of nonlinear effects. For example, particle trajectories that would be stable in a real storage ring may appear to be unstable if the storage ring is modelled using non-symplectic maps, and this can lead to an inaccurate estimate of the dynamic aperture and the beam lifetime.

## 5.5 Symplectic transfer maps

Real accelerators are often sufficiently complex that it is necessary to construct concise approximate representations of the transfer maps for the various components: fully detailed and accurate transfer maps are usually too demanding in terms of computer processing speed and memory capacity to be of practical use in computational models. Expanding the transfer map as a power series in the dynamical variables provides a convenient representation of a transfer map, in terms of a set of coefficients for the power series. However, we have seen that the power series that result from an expansion of a nonlinear transfer map often have an infinite number of terms. It may be possible in some cases simply to truncate the power series at some point; however, we have seen that when we do so, the resulting power series is often not symplectic. Symplecticity is an important property of some accelerator systems, and the loss of symplecticity can lead to a model producing misleading results.

To address this issue, a number of techniques have been developed for representing symplectic maps in convenient, concise forms. For example, it is possible to construct a power series map that



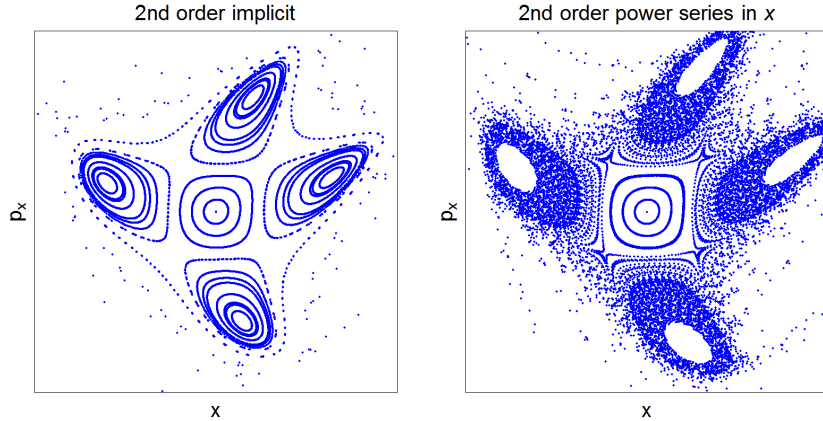


**Fig. 18:** Phase space portraits for a simple storage ring containing a sextupole magnet. The lattice is the same in both cases, but in the left-hand plot the phase space portrait is constructed using symplectic maps, while non-symplectic maps are used to construct the plot on the right.

is of finite order, symplectic, and approximates (to a specified degree) a given symplectic power series map with an infinite number of terms. This approach has the additional advantage that a power series representation is *explicit*: all that is required to apply the map is to substitute particular values of the dynamical variables into the given expressions. However, finite-order symplectic power series are not easy to construct, and may have limited accuracy unless extended to very high order, and alternative techniques may be worth investigating. Examples include the use of mixed-variable generating functions (see Appendix B) and Lie transformations (Appendix C): both of these are powerful techniques, but provide *implicit* representations of transfer maps in the sense that an additional set of equations needs to be solved (usually numerically) each time the map is applied. This can make these techniques cumbersome to implement, computationally expensive, and may limit accuracy.

As an example of a technique for constructing a symplectic map in the form of a power series, we shall discuss the “kick” approximation that is widely used for modelling multipole magnets in accelerators. The technique can be applied to multipoles of any order; but for simplicity, we shall consider just a sextupole magnet. As usual, and again for simplicity, we consider only motion in one degree of freedom, though the technique that we develop can readily be extended to include additional degrees of freedom.

We start with the equations of motion for a particle moving through the sextupole:

$$\frac{dx}{ds} = p_x, \quad (89)$$

$$\frac{dp_x}{ds} = -\frac{1}{2}k_2x^2. \quad (90)$$

Since these equations of motion can be derived using Hamilton’s equations, the solution must be symplectic. Unfortunately, the equations do not have an exact solution in terms of elementary functions. However, in the approximation that  $p_x$  is constant, we can solve Eq. (89); and in the approximation that  $x$  is constant we can solve Eq. (90). We therefore split the integration into three steps, making the one or the other approximation at each step. If the total length of the magnet is  $L$ , we take the first step over  $0 \leq s < L/2$ , making the approximation that  $p_x$  is constant, so that the transfer map is:

$$x_1 = x_0 + \frac{L}{2}p_{x0}, \quad p_{x1} = p_{x0}. \quad (91)$$

Then we make the approximation that  $x$  is constant, taking  $x = x_1$ , and integrate Eq. (90) over the full

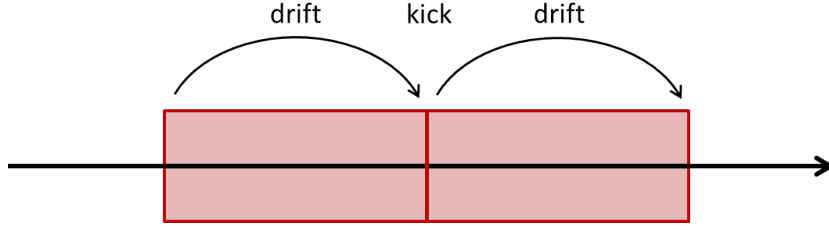


**Fig. 19:** Drift–kick–drift approximation for constructing a symplectic transfer map for a multipole magnet.

length of the magnet:

$$x_2 = x_1, \quad p_{x2} = p_{x1} - \frac{1}{2}k_2Lx_1^2. \quad (92)$$

Finally, we again make the approximation that  $p_x$  is constant, and integrate Eq. (89) over  $L/2 < s \leq L$ :

$$x_3 = x_2 + \frac{L}{2}p_{x2}, \quad p_{x3} = p_{x2}. \quad (93)$$

Because of the way that we have approximated the equations of motion, each of the transfer maps expressed in Eqs. (91), (92) and (93) is symplectic. The (approximate) solution (91)–(92) to the equations of motion (89) and (90) is an example of a *symplectic integrator*. For obvious reasons, this particular integrator is known as a “drift–kick–drift” approximation: see Fig. 19. In this case, the approximation can work well if the length of the sextupole is short (compared to the betatron wavelength). However, by splitting the integration into smaller steps, it is possible to obtain better approximations. Using techniques from classical mechanics, it can be shown that by splitting a multipole in particular ways, that is with certain combinations of drifts of varying lengths and kicks of different strengths, it is possible to minimise the error for a given number of integration steps: simply dividing a multipole into steps of equal length and applying kicks of equal strength is not usually the best solution.

## 5.6 Analysis techniques for nonlinear dynamics

Power series maps are useful for particle tracking, but do not give much insight into the dynamics of a given nonlinear system. To develop a deeper understanding (for example, to determine the impact of individual resonances in a storage ring) more powerful techniques are needed. There are two approaches that are widely used in accelerator physics: perturbation theory [5–7], and normal form analysis [8–10]. In both these techniques, the goal is to construct a quantity that is invariant under application of the transfer map. Unfortunately, in both cases the mathematics is complicated and fairly cumbersome, and we do not discuss the details here. However, by way of illustration, consider the case of a simple storage ring containing a single sextupole in each periodic cell. Normal form analysis provides an expression for the betatron action  $J_x$  of a particle in terms of the phase  $\phi_x$  in this case [11]:

$$J_x \approx I_0 - \frac{k_2L}{8}(2\beta_x I_0)^{3/2} \frac{(\cos(3\mu_x/2 + 2\phi_x) + \cos(\mu_x/2))}{\sin(3\mu_x/2)} + O(I_0^2), \quad (94)$$

where  $I_0$  is a constant (an invariant of the motion),  $\phi_x$  is the angle variable, and  $\mu_x$  is the phase advance per cell. Recall that the cartesian variables  $x, p_x$  are related to the action–angle variables  $J_x, \phi_x$  through Eqs. (12) and (13).

Note that the second term in the expression (94) for  $J_x$  becomes very large when  $\mu_x/2\pi$  is close to a third integer: this is the indication of a resonance. For linear motion, the action will be constant. The sextupoles in the lattice introduce some nonlinearity, which leads to a variation of the action as a particle moves around the ring (i.e. as the phase  $\phi_x$  increases). The variation in the action becomes very large

close to a third-order resonance. Although higher-order resonances may also be driven by the sextupoles, these are not shown in the expression in Eq. (94), which is based on normal form analysis carried out only up to a given order.

The phase space distortion (related to the variation in the betatron action as a function of angle) is illustrated in Fig. 20. Results from particle tracking (using a symplectic integrator) are shown as point on the plot; the variation in the action described by normal form analysis in Eq. (94) is shown as a solid line. Although there is not exact agreement, the normal form analysis does give a reasonable description of the dynamics, at least at low amplitude. Very large distortions (resulting from motion close to a resonance, or from a strongly-driven resonance, or at large amplitude) are difficult to describe analytically.

### 5.7 Tune shift with amplitude

Close inspection of the plots in Fig. 20 reveals another effect, in addition to the obvious distortion of the phase space ellipses: the phase advance per turn (i.e. the tune) varies with increasing betatron amplitude. This effect is known simply as *tune shift with amplitude*. Normal form analysis and perturbation theory can both be used to obtain estimates for the size of the tune shift with amplitude, in terms of the coefficients of a series expansion for the tune in terms of the action:

$$\nu_x = \nu_{x0} + \left. \frac{\partial \nu_x}{\partial J_x} \right|_{J_x=0} J_x + \frac{1}{2} \left. \frac{\partial^2 \nu_x}{\partial J_x^2} \right|_{J_x=0} J_x^2 + \dots \quad (95)$$

Note that in general, the tune in each plane (transverse horizontal and vertical) depends not just on the action in the corresponding plane, but also on the action in the opposite plane. One consequence of the fact that the motion (under appropriate conditions) is symplectic is that the horizontal tune shift with vertical amplitude is equal, or at least very close to, the vertical tune shift with horizontal amplitude.

Where the nonlinearity in a storage ring arises from a single sextupole in each periodic cell, the lowest order term in the expansion in Eq. (95) is second-order in the action. An octupole, however, does have a first-order tune shift with amplitude, given by:

$$\nu_x = \nu_{x0} + \frac{k_3 L \beta_x^2}{16\pi} J_x + O(J_x^2), \quad (96)$$

where  $k_3 L$  is the integrated strength of the octupole, integrated over the length of the octupole:

$$k_3 L = \frac{q}{P_0} \int_0^L \frac{\partial^3 B_y}{\partial x^3} ds. \quad (97)$$

The tune shift with amplitude in a storage ring with a single octupole per cell becomes obvious if we construct a phase space portrait by tracking particles through a small number of cells: an example (for 30 cells) is shown in Fig. 21.

Tune shift with amplitude helps to explain the “islands” that we observed appearing in the phase space portraits for a storage ring with a single sextupole per periodic cell, see Fig. 10. The islands (closed loops around points away from the origin in phase space) are associated with resonances, and appear at amplitudes where the phase advance is  $2\pi$  times a simple ratio of two integers, and where the transfer map contains an appropriate driving term for a resonance at the corresponding phase advance. The number of islands is determined by the denominator of the ratio of integers, and the width of the islands depends on the size of the tune shift with amplitude, and on the strength of the driving term.

For example, if we consider a one-turn map with a single octupole magnet and a linear map tuned for a phase advance close to a 4<sup>th</sup> order resonance, we observe four stable islands in the phase space as shown in Fig. 22 (left). The tune shift with amplitude is illustrated in Fig. 22 (right), showing the tunes of the tracked particles as a function of their initial action ( $2J_x$ ). Particles with small amplitude

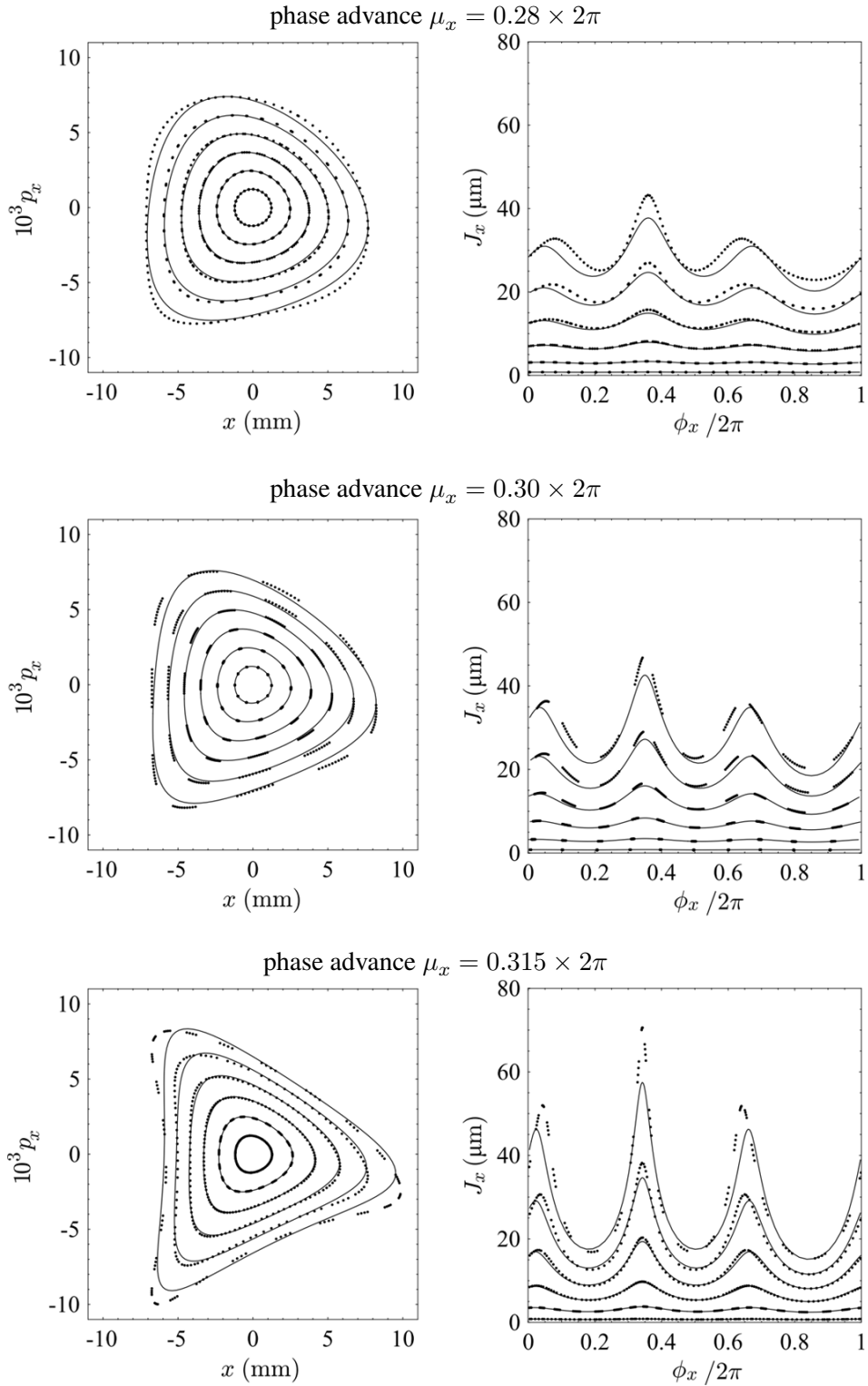


**Fig. 20:** Comparison between phase space portraits constructed by particle tracking, and by application of normal-form analysis. Each plot shows the horizontal phase space for a particle moving through a lattice with a single sextupole in each periodic cell, with phase advance per cell equal to  $\mu_x$ . The points are calculated by particle tracking, using a symplectic integrator. The lines are constructed from Eq. (94), based on normal form analysis.

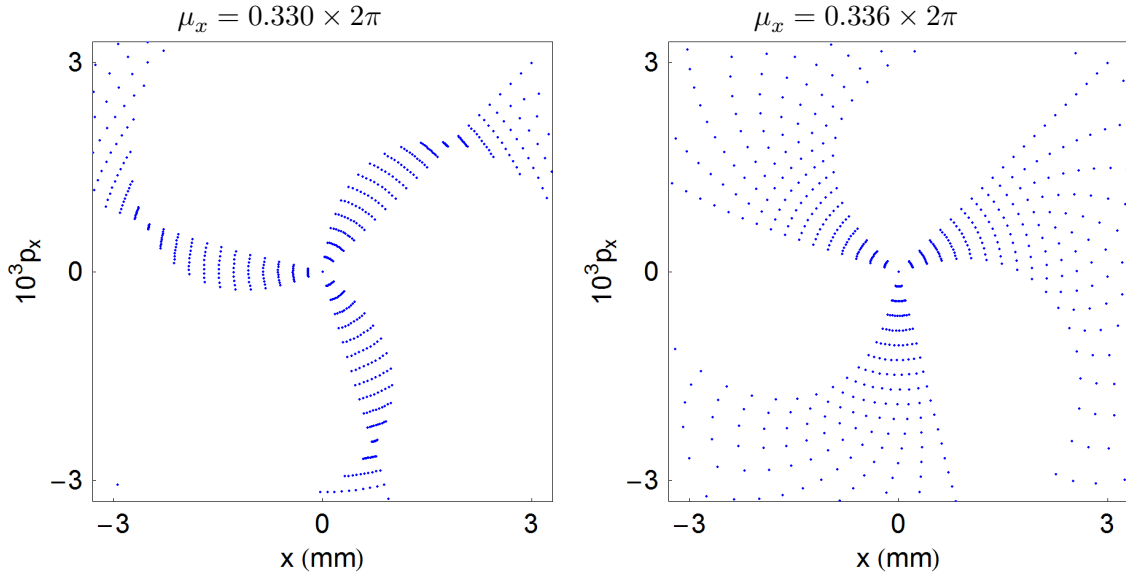


**Fig. 21:** Tune shift with amplitude: the phase space portraits are constructed by tracking particles with different betatron amplitudes through 30 periodic cells, with a single nonlinear element (an octupole) in each cell. The phase advance per cell varies depending on the betatron amplitude, and on the phase advance per cell in the limit of zero amplitude (shown above each plot).

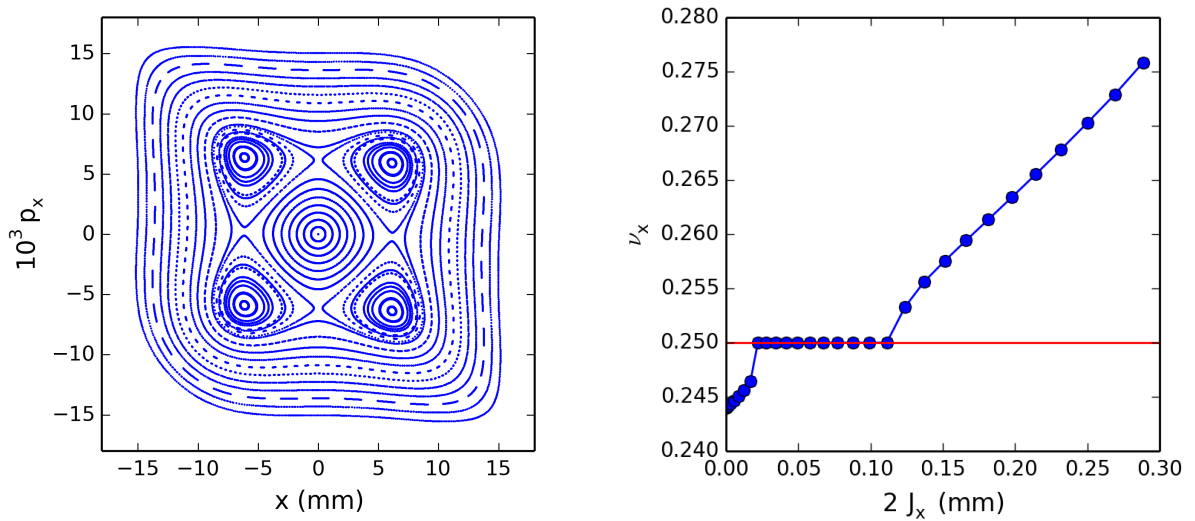


**Fig. 22:** Phase space portrait (left) and horizontal tunes as a function of the initial particle action (right) for a one-turn map consisting of an octupole magnet and a linear map tuned to a phase advance of  $\mu_x = 0.244 \times 2\pi$ .

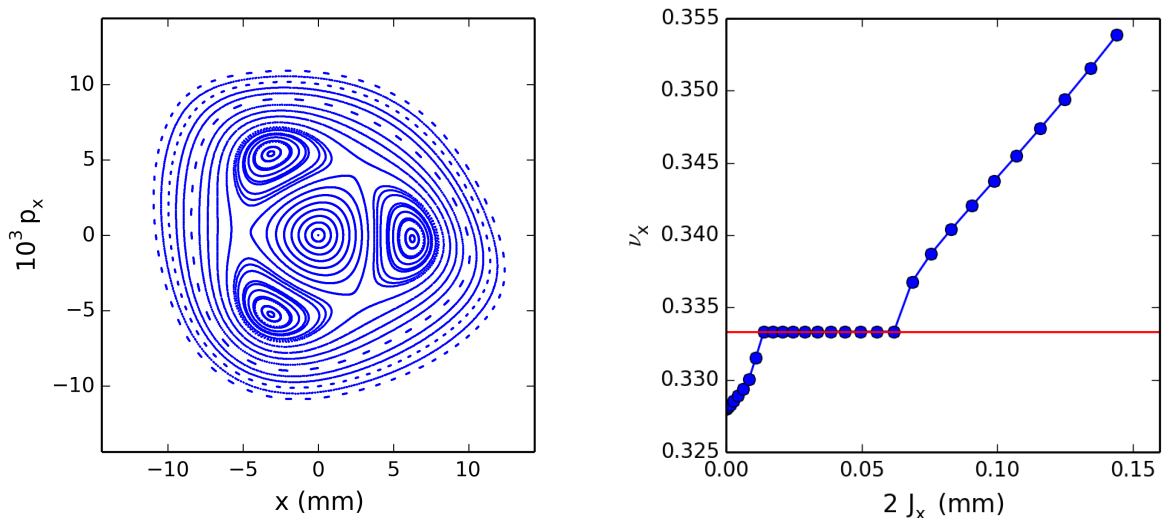


**Fig. 23:** Phase space portrait (left) and horizontal tunes as a function of the initial particle action (right) for a one-turn map consisting of a sextupole magnet, an octupole magnet and a linear map tuned to a phase advance of  $\mu_x = 0.328 \times 2\pi$ .

have tunes below the resonance. For large amplitudes, particles have tunes above the resonance and their tunes increase linearly with action. Particles trapped in the resonance islands have (on average) a tune locked to the resonance condition. As mentioned above, the width of the resonance islands depends on the tune shift with amplitude and on the resonance strength. This is also demonstrated in another case, where we consider a one-turn map consisting of a sextupole, an octupole and a linear map tuned to a phase advance of  $\mu_x = 0.328 \times 2\pi$  (i.e. close to the 3<sup>rd</sup> order resonance) as shown in Fig. 23. Here the phase space exhibits three stable islands. Note that the octupole induces a large tune shift with amplitude, which stabilises the particle motion at the resonance as it moves the particle tune out of the resonance for increasing amplitudes. For comparison, without the octupole and thus with a much smaller tune shift with amplitude, particles get lost at the same resonance as we have seen in Fig. 10.

## 6 Dynamic aperture and Frequency Map Analysis

The techniques we have mentioned for the analysis of nonlinear effects, perturbation theory and normal form analysis, are based on the existence of constants of motion in the presence of nonlinear perturbations. For linear motion in accelerators, there are constants of motion given by the action variables; for example, in the horizontal plane:

$$2J_x = \gamma_x x^2 + 2\alpha_x x p_x + \beta_x p_x^2. \quad (98)$$

In a periodic lattice, the Courant–Snyder parameters have the same periodicity as the lattice itself, and the action  $J_x$  remains constant as a particle moves along the beamline. When nonlinear components are present (e.g. sextupoles) then the betatron action can vary with position; but normal form analysis may still identify constants of the motion. An example is the quantity  $I_0$  in Eq. (94).

It is not obvious, however, that constants of motion can exist in the presence of nonlinear perturbations. The fact that they can is a consequence of the *Kolmogorov–Arnold–Moser (KAM) theorem* [12]. The KAM theorem expresses the general conditions for the existence of constants of motion in nonlinear Hamiltonian systems, and is of particular significance in accelerator beam dynamics since it tells us that resonances do not invariably result in the immediate loss of stability. Resonances will usually

tend to drive the amplitudes of particles with a particular tune to large amplitudes; however, if the tune shift with amplitude is sufficiently large, then it is possible for there to be a region of stable motion in phase space at amplitudes significantly larger than that at which resonance occurs. In simple terms, the resonance occurs over a limited range of betatron amplitudes: at lower or larger amplitudes, the tune shift with amplitude moves the particle motion away from the resonance, meaning that the motion can again be stable. However, the overlapping of two resonances is associated with a transition from regular to chaotic motion, which is certainly associated with instability. The parameter range over which the particle motion becomes chaotic is described by the *Chirikov criterion* [13].

We have so far focused on motion in one degree of freedom. In that case (for example, in the phase space portraits shown in Fig. 10) instability occurred when the oscillation amplitude exceeded a certain value. In multiple degrees of freedom, a new phenomenon occurs: *Arnold diffusion* [14]. This refers to the fact that there can be regions of phase space where motion with large amplitude is stable (associated with the existence of constants of the motion), while regions of chaotic motion exist at *smaller* amplitudes. In storage rings, for example, this means that particle trajectories with initially small amplitudes can be unstable, even if trajectories with much larger amplitudes are stable.

One way of studying Arnold diffusion in dynamical systems is through the use of *frequency map analysis* (FMA) [15, 16]. This applies a technique known as “numerical analysis of the Fourier frequencies” to particle tracking data, either from a simulation or collected experimentally, to determine with high precision the tunes associated with different particle trajectories. The strengths of different resonances can be seen by plotting points in tune space, with diffusion rates shown by different colours: an example for the Advanced Light Source (ALS) at Lawrence Berkeley National Laboratory (LBNL) is shown in Fig. 24. The FMA reveals several properties of the nonlinear dynamics in a very visual way, such as the detuning with amplitude, the onset of chaos in co-ordinate space and the corresponding areas in tune space, resonances crossed by the tune footprint, areas of large diffusion, and so on. The boundary of the stable region in co-ordinate space is known as the *dynamic aperture*.

A large dynamic aperture is needed both for good efficiency of injection of the beam into a storage ring, and for good lifetime of the stored beam. Although the beam may be much smaller than the dynamic aperture, scattering processes within the beam can result in particles acquiring large amplitude betatron or synchrotron oscillation amplitudes, which may take them outside the dynamic aperture. When that happens, the particles will be lost from the machine. Achieving sufficiently large dynamic aperture is typically one of the biggest challenges in the design of modern light sources, due to their inherent strong nonlinearities.

## 7 Summary and further reading

The effects of nonlinear dynamics impact a wide variety of accelerator systems, including single-pass systems (such as bunch compressors) and multi-turn systems (such as storage rings). It is possible to model nonlinear dynamics in a given component or section of accelerator beamline by representing the transfer map as a power series. Power series provide a convenient (explicit) representation of a transfer map for modelling nonlinear effects and for simple analysis of nonlinear dynamics in accelerators. However, nonlinear transformations associated with particular accelerator components can usually only be represented with complete accuracy by power series with an infinite number of terms: in practice, it is necessary to truncate the power series, i.e. to drop terms above some order in the dynamical variables.

Conservation of phase space volumes, expressed in Liouville’s theorem, is an important feature of the beam dynamics in many systems; one example is the conservation of the beam emittances (in the absence of synchrotron radiation and certain collective effects). To conserve phase space volumes, transfer maps must be symplectic; but in general, truncated power series maps are not symplectic. There are alternative representations that guarantee symplecticity, but these representations are usually less convenient. For example, while power series maps are explicit in that they require only the substitution

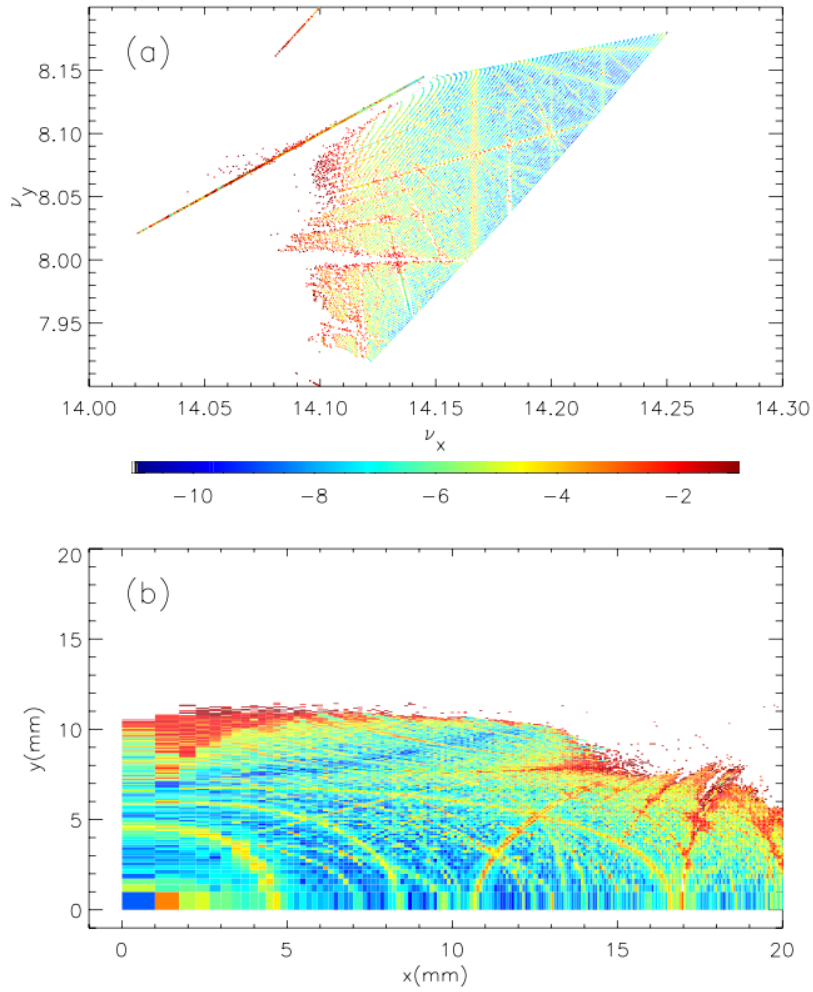


**Fig. 24:** Example of frequency map analysis for the Advanced Light Source at Lawrence Berkeley National Laboratory, obtained from analysis of particle tracking data [17].

of values into given expressions, symplectic maps are often implicit, requiring the numerical solution of a set of equations each time they are applied. Techniques do exist, however, that allow the construction of a symplectic transfer map in an explicit form. An example is the “drift–kick–drift” approximation for a multipole magnet. A map constructed using such a technique is known as an explicit symplectic integrator.

Common features of nonlinear dynamics in accelerators include phase space distortion, tune shifts with amplitude, resonances, and instability of particle trajectories at large amplitudes (limits on dynamic aperture and energy acceptance). Analytical methods such as perturbation theory and normal form analysis can be used to estimate the impact of nonlinear perturbations in terms of quantities such as resonance strengths and tune shift with amplitude. Analytical studies are often supported by tracking simulations and by numerical techniques, such as frequency map analysis, that can provide powerful tools for characterising effects of nonlinear dynamics in accelerators, including tune shifts and resonance strengths. Understanding (and correcting, where necessary and possible) nonlinear effects in accelerators is important for optimising their performance, for example in achieving a good beam lifetime in a storage ring.

As we mentioned in the introduction, there are many publications that cover the material discussed



in these notes. Linear optics, and some of the general principles and techniques of nonlinear dynamics, are covered in (for example) [1–3]. Many of the tools of nonlinear dynamics are based on standard techniques in classical mechanics: this includes the use of mixed-variable generating functions for the representation of symplectic maps, and canonical perturbation theory. Such methods are widely covered in standard text on classical mechanics, for example [5, 18]. Perturbation theory applied to accelerator physics is discussed in [6, 7, 19]. Normal form analysis has proved a powerful tool in many situations, and is developed in [8–10]. Symplectic integration is an important topic in nonlinear dynamics in accelerators, and is discussed in [20–23]; a more general text is [24]. Frequency map analysis is reviewed and discussed in [16, 17, 26, 28].

## Appendices

### A Mixed-variable generating functions

A mixed-variable generating function represents a transfer map (or, more generally, a canonical transformation) in the form of a function of initial and final values of the phase space variables. There are different kinds of generating function. A mixed-variable generating function of the third kind (in Goldstein’s nomenclature [5]) is expressed as a function of the initial momenta  $\vec{p}$  and final co-ordinates  $\vec{X}$  (i.e. the momenta before applying the transformation, and the co-ordinates after applying the transformation):

$$F_3 = F_3(\vec{X}, \vec{p}). \quad (\text{A.1})$$

The final momenta  $\vec{P}$  and initial co-ordinates  $\vec{x}$  are obtained by:

$$\vec{x} = -\frac{\partial F_3}{\partial \vec{p}}, \quad \text{and} \quad \vec{P} = -\frac{\partial F_3}{\partial \vec{X}}. \quad (\text{A.2})$$

As an example, consider the mixed-variable generating function in one degree of freedom:

$$F_3 = -Xp_x + \frac{1}{2}Lp_x^2. \quad (\text{A.3})$$

Applying (A.2) leads to the equations:

$$x = X - Lp_x, \quad \text{and} \quad P_x = p_x. \quad (\text{A.4})$$

In this case, the equations are easily (trivially!) solved to give explicit expressions for  $X$  and  $P_x$  in terms of  $x$  and  $p_x$ :

$$X = x + Lp_x, \quad \text{and} \quad P_x = p_x. \quad (\text{A.5})$$

We see that the function  $F_3$  in Eq. (A.3) is a mixed-variable generating function for a drift space. In more general cases, the equations (A.2) need to be solved numerically each time the transfer map is applied.

### B Lie transformations

Lie transformations make use of the fact that the equations of motion for a particle in an electromagnetic field can be written in the form:

$$\frac{d\vec{x}}{ds} = - :H : \vec{x}, \quad (\text{B.1})$$

where  $\vec{x} = (x, p_x, y, p_y, z, \delta)$  is the phase space vector, and  $:H :$  is a Lie (differential) operator:

$$:H := \sum_{i=1}^3 \frac{\partial H}{\partial x_i} \frac{\partial}{\partial p_i} - \frac{\partial H}{\partial p_i} \frac{\partial}{\partial x_i}. \quad (\text{B.2})$$

The precise form of the function  $H = H(\vec{x})$  (the Hamiltonian) depends on the field through which the particle is moving.

Formally, a solution to (B.1) can be written:

$$\vec{x}|_{s=L} = e^{-L:H:} \vec{x}|_{s=0}, \quad (\text{B.3})$$

where the exponential of the Lie operator is defined by the usual series expansion for an exponential:

$$e^{-L:H:} = 1 - L:H: + \frac{L^2}{2} :H:^2 - \frac{L^3}{3!} :H:^3 + \dots \quad (\text{B.4})$$

The operator  $e^{-L:H:}$  is known as a *Lie transformation*. As a simple example, consider the Hamiltonian:

$$H = \frac{1}{2}p_x^2 + \frac{1}{2}k_1x^2. \quad (\text{B.5})$$

Applying the Lie operator  $:H:$  to the variables  $x$  and  $p_x$  gives:

$$:H:x = -p_x, \quad (\text{B.6})$$

$$:H:p_x = k_1x. \quad (\text{B.7})$$

A further application then gives:

$$:H:^2x = -k_1x, \quad (\text{B.8})$$

$$:H:^2p_x = -k_1p_x, \quad (\text{B.9})$$

and so on. Then, we find that the Lie transform of  $x$  is:

$$e^{-L:H:}x = x + Lp_x - \frac{1}{2}k_1L^2x - \frac{1}{6}k_1L^3p_x + \dots \quad (\text{B.10})$$

Collecting terms in  $x$  and  $p_x$ , and making use of the series expansions of the trigonometric functions, we find that:

$$e^{-L:H:}x = x \cos(\sqrt{k_1}L) + p_x \frac{\sin(\sqrt{k_1}L)}{\sqrt{k_1}}. \quad (\text{B.11})$$

Similarly, we find:

$$e^{-L:H:}p_x = p_x - k_1Lx - \frac{1}{2}k_1L^2p_x + \frac{1}{6}k_1^2L^3x + \dots \quad (\text{B.12})$$

which can be written:

$$e^{-L:H:}p_x = p_x \cos(\sqrt{k_1}L) - x\sqrt{k_1} \sin(\sqrt{k_1}L). \quad (\text{B.13})$$

The Hamiltonian in Eq. (B.5) leads to the Lie transformation for a quadrupole (in one degree of freedom).

In the above example, although the Lie transformation led to transformations for the dynamical variables in terms of infinite series, it was possible to express the series in finite form using standard trigonometric functions. Unfortunately, this is not generally the case, and applying a Lie transformation to a dynamical variable generally leads to an infinite power series that cannot be written exactly in finite form. However, the power of Lie transformations lies in the fact that there are known mathematical rules for combining and manipulating Lie transformations, and that for any *generator*  $g = g(\vec{x})$  the Lie transformation  $e^{g:}$  represents a symplectic map. This makes it possible to use Lie transformations for the analysis of nonlinear dynamics in a given system (such as a particle accelerator) using finite expressions for the generators, rather than infinite series.

## References

- [1] S.Y. Lee, *Accelerator Physics* (World Scientific, 3rd edition, 2011).
- [2] A. Wolski, *Beam Dynamics in High Energy Particle Accelerators* (Imperial College Press, 2014).
- [3] H. Wiedemann, *Particle Accelerator Physics* (Springer, 4th edition, 2015).
- [4] D. Robin, C. Steier, J. Safranek, W. Decking, “Enhanced performance of the ALS through periodicity restoration of the lattice,” Proceedings of EPAC2000, Vienna, Austria (2000), pp. 136–140.
- [5] H. Goldstein, C.P. Poole Jr., J.L. Safko, *Classical Mechanics* (Pearson, 3rd edition, 2013).
- [6] R.D. Ruth, “Single particle dynamics and nonlinear resonances in circular accelerators”, in *Nonlinear dynamics aspects of particle accelerators*, Lecture Notes in Physics, Vol. 247 (Springer, 1986), pp. 37–63.
- [7] R.D. Ruth, “Single particle dynamics in circular accelerators”, Tech. Rep. SLAC–PUB–4103, (Stanford Linear Accelerator Center, 1986).
- [8] A.J. Dragt and J.M. Finn, “Normal form for mirror machine Hamiltonians”, *Journal of Mathematical Physics* 20 (1979), pp. 2649–2660.
- [9] F. Neri and A.J. Dragt, “Analysis of tracking data using normal forms”, Proceedings of the First European Particle Accelerator Conference, Rome, Italy (1988), pp. 675–677.
- [10] É. Forest, *Beam Dynamics: A New Attitude and Framework* (CRC Press, 1998).
- [11] Ibid. [2], pp. 373–384.
- [12] V.I. Arnold, *Mathematical methods of classical mechanics* (Springer, 2nd edition, 1989).
- [13] B.V. Chirikov, “A universal instability of many-dimensional oscillator systems”, *Physics Reports* 52, 5 (1979), pp. 263–379.
- [14] V.I. Arnold, “Instability of dynamical systems with several degrees of freedom”, *Soviet Mathematics* 5 (1964), pp. 581–588.
- [15] J. Laskar, “The chaotic motion of the solar system: a numerical estimate of the size of the chaotic zones”, *Icarus* 88 (1990), pp. 266–291.
- [16] J. Laskar, “Frequency map analysis of a Hamiltonian system”, Proceedings of “Nonlinear dynamics in particle accelerators: theory and experiments”, Arcidosso, Italy (1994), pp. 160–169.
- [17] J. Laskar, “Frequency map analysis and particle accelerators”, Proceedings of the 2003 Particle Accelerator Conference, Portland, OR, USA (2003), pp. 378–382.
- [18] L.N. Hand and J.D. Finch, *Analytical mechanics*, (Cambridge University Press, 1999).
- [19] S.G. Peggs and R.M. Talman, “Nonlinear problems in accelerator physics”, *Ann. Rev. Nucl. Part. Sci.* 36 (1986), pp. 287–325.
- [20] “A canonical integration technique”, *IEEE Transactions on Nuclear Science*, NS-30 (4) (1983), pp. 2669–2671.
- [21] “Geometric integration for particle accelerators”, *J. Phys. A: Math. Gen.* 39 (19) (2006), pp. 5321–5377.
- [22] “Fourth-order symplectic integration”, *Physica D*, 43 (1990).
- [23] “Construction of higher-order symplectic integrators”, *Phys. Lett. A*, 150 (1990).
- [24] E. Hairer, C. Lubich, G. Wanner, *Geometric numerical integration*, (Springer Series in Computational Mathematics, 2006).
- [25] H. Bartosik, G. Arduini, Y. Papaphilippou, “Optics considerations for lowering transition energy in the SPS”, Proceedings of the 2011 International Particle Accelerator Conference, San Sebastian, Spain (2011), pp. 619–621.
- [26] Y. Papaphilippou, “Detecting chaos in particle accelerators through the frequency map analysis method”, *Chaos: An Interdisciplinary Journal of Nonlinear Science* 24, 024412 (2014).
- [27] M.A. Palmer et al., “The conversion and operation of the Cornell Electron Storage Ring as a test

accelerator (CesrTA) for damping rings research and development”, Proceedings of PAC09, Vancouver, BC, Canada (2009), pp. 4200–4204.

- [28] J. Laskar, “Introduction to frequency map analysis”, Proceedings of the NATO Advanced Studies Institute on “Hamiltonian systems with three or more degrees of freedom”, S’Agaro, Spain (1995), p. 134–150.